ON A VIBRATION RESPONSE OF A PLATE SUBMERGED IN FLUID

SUYUN CAO

ON A VIBRATION RESPONSE OF A PLATE SUBMERGED IN FLUID

BY

© SUYUN CAO, B.ENG., M.SCI.

A THESIS SUBMITTED TO THE SCHOOL OF GRADUATE STUDIES IN PARTIAL FULFILLMENT OF THE REQUIREMENTS FOR THE DEGREE OF MASTER OF ENGINEERING

MAY 1994

FACULTY OF ENGINEERING AND APPLIED SCIENCE

MEMORIAL UNIVERSITY OF NEWFOUNDLAND

ST. JOHN'S NEWFOUNDLAND CANADA

ISBN 0-315-91595-1

Abstract

This study deals with the dynamic characteristics of plates submerged in water using analytical and experimental methods. The plates considered have two kinds of boundary conditions, one with clamped-free-clamped-free(CFCF) supports, another with simple-free-simple-free(SFSF) supports. They are submerged in water at different depths.

For the experimental study, modal testing of the two plates is carried out in air and in water. The effect of the depth of submergence of the plate is investigated. The simply supported condition was simulated by using a notched plate with a clamped end and the finite element software ABAQUS is used to determine the dimensions of the notch. The appropriateness of the tested plates as models of the CFCF and SFSF plates is verified. The added mass factor, which is used to account for the decrease in natural frequencies, and the increase in modal damping ratios for the vibrating plates submerged in water have been evaluated for the first five modes. The effect of the plate boundary conditions on the vibration of plates in water is also investigated.

In the analytical study, a thin plate undergoing a flexural bending vibration in a body of homogeneous, incompressible and inviscid fluid whose motion is irrotational, is considered. The governing equation for the surface displacement of the plate-fluid system is derived. In the effort to solve the velocity potential, the general linearized fluid free surface boundary condition is applied. The relationship between the added mass and the depth of submergence above and below the plate is established.

The analytical solution is applied to the CFCF and SFSF plates submerged in

water, and the experimental and analytical studies on the added mass due to the presence of fluid are compared. The maximum difference between the measured and the predicted added mass factors is found to be within 7.916%.

Acknowledgments

The author would like to appreciate the support and encouragement from individuals in the program of Master of Engineering. Particular thanks are due:

(a) Dr. M. R. Haddara and Dr. A. S. J. Swamidas, Professors of ocean engineering, for their supervision, guidance and financial support throughout this program.

(b) Faculty of Engineering and Applied Science and the School of Graduate Studies for their financial support of graduate fellowship and teaching assistantship.

(c) Mr. A. Bursey for his help in preparing the experimental devices.

(d) Mr. J. Andrews, Mr. H. Dye and other staff in the Machine Shop for their technical services and suggestions in manufacturing the tank and setup.

(e) Finally, her family members, especially her husband and parents, for their deep understanding and encouragement.

Contents

List of Figures

List of Tables

List of Symbols

x,y,z - Cartesian coordinates.

t - time in seconds.

a, b, h - length, breadth and thickness of the plate, m.

L_1, L_2 - length, width of the water tank, m.

h_1, h_2 - fluid level above the upper surface and below the lower surfaces of the submerged plate, respectively.

ρ_f - fluid density, kg/m^3.

ρ - density of the plate material, kg/m^3.

$m = \rho h$ - mass of the plate per unit area, kg/m^2.

E - elastic modulus, N/m^2.

ν - Poisson's ratio.

$D = \frac{Eh^3}{12(1-\nu^2)}$ - flexural rigidity of the plate, Nm.

g - gravity acceleration, m/s^2.

μ - plane wave number.

k - modal wave number.

β, β' - constants.

W(x,y,t) - bending displacement of the plate, measured upward from its static equilibrium position.

$\phi(x, y, z, t)$ - velocity potential.

$p_L(x, y, t)$ - fluid dynamic pressure on the plate-fluid interface S_L, N/m^2.

$p_U(x, y, t)$ - fluid dynamic pressure on the plate-fluid interface S_U, N/m^2.

p - dynamic pressure at any point in fluid, N/m^2.

f_{air} - natural frequency of the plate in air, Hz.

f_{fluid} - natural frequency of the plate submerged in fluid, Hz.

ω_{air} - natural frequency of the plate in air, rad/sec.

ω_{fluid} - natural frequency of the plate submerged in fluid, rad/sec.

ω - frequency of the wave motion on the free fluid surface, rad/sec.

m^* - added mass per unit area, kg/m^2.

m_1^* - contribution to the added mass from the fluid above the plate, kg/m^2.

m_2^* - contribution to the added mass from the fluid below the plate, kg/m^2.

n - number of degrees-of-freedom.

γ^2 - coherence function.

$s = \delta + jw$ - Laplace variable.

$[M]$ - $n \times n$ mass matrix.

$[C]$ - $n \times n$ damping matrix.

$[K]$ - $n \times n$ stiffness matrix.

$\{x(t)\}$ - $n \times 1$ vector of displacements.

$\{\dot{x}(t)\}$ - $n \times 1$ vector of velocities.

$\{\ddot{x}(t)\}$ - $n \times 1$ vector of accelerations.

$\{f(t)\}$ - $n \times 1$ vector of forces.

{q(t)} - $n \times 1$ vector of displacements in modal space.

$\{X(s)\}$ - $n \times 1$ vector of displacements in Laplace domain.

$\{F(s)\}$ - $n \times 1$ vector of forces in Laplace domain.

$[H(s)]$ - transfer function matrix.

$[U]$ - mode shape matrix, $[U] = [U_1, U_2, \ldots . U_n]$.

$[\overline{M}]$ - generalized mass matrix, $[\overline{M}] = [U]^T[M][U]$.

$[\overline{C}]$ - generalized damping matrix, $[\overline{C}] = [U]^T[C][U]$.

$[\overline{K}]$ - generalized stiffness matrix, $[\overline{K}] = [U]^T[K][U]$.

$\{P(t)\}$ -$n \times 1$ vector of forces in modal space, $\{P(t)\} = [U]^T\{f(t)\}$.

$[A_r]$ - the r-th residual matrix.

ω_r - the r-th complex frequency, rad/sec.

$P_{ik}(j\omega)$ - lower residual.

$Q_{ik}(j\omega)$ - upper residual.

Chapter 1

Introduction

In a large class of dynamic problems, the structure either contains or is surrounded by fluid. Examples include safety analysis of nuclear reactors, seismic analysis of large liquid storage tanks, dynamics of ships, and submarines. In these problems, the structural displacement modifies the flow field, which in turn affects the structural responses. Generally, these are categorized as fluid-structure interaction problems.

In fluid-structure interaction problems, natural frequencies, damping ratios and mode shapes of a structure are different from those in air. The prediction of these changes due to the presence of fluid is important, as this makes it possible for a designer to select appropriate structural parameters, geometry, damping coatings, etc, to suppress structural vibration.

Many studies on the fluid-structure interaction problems have been carried out by analytical, numerical and experimental methods. Studies performed by Rayleigh[1877], Lamb[1921], Peake and Thurston[1954], Dowell and Voss[1963], Qaisi[1988] and Robinson and Palmer[1990] presented analytical solutions for predicting the fluid effect on the vibration of simple structures such as circular or rectangular plates. Numerical studies carried out by Marcus[1978], Volcy et al.[1979], Muthuveerappan[1978, 1979,

1980] and Everstine[1991] investigated complex structures and/or complex boundary conditions of structures and fluid. Reports of experimental studies on submerged cantilevered plates[Lindholm, 1965] [Budipriyanto, 1993], on perforated plates[De Santo, 1981], and on a cylindrical structure[Randall, 1985], have been published. In general, these studies have exposed the mechanism of fluid-structure interaction problems and/or presented methodologies to estimate the fluid effect on the vibration of submerged structures. The fluid effect on a structure can be considered as an added mass for lower modes, and as an added mass and an added damping for higher modes. However, neither analytical nor experimental study which investigates the effect of the depth of submergence on a rectangular plate oriented horizontally has been reported before. Also, there is no reference in the open literature which investigates experimentally the effect of boundary conditions on the vibration of rectangular plates submerged in fluid.

This thesis presents analytical and experimental studies on rectangular plates submerged in water at different depths with the intent of gaining an insight into the mentioned subjects. The plates have two different boundary conditions, one has clamped-free-clamped-free(CFCF) supports and the other has simple-free-simple-free(SFSF) supports. The organization of the study is made in the following manner:

Literature review of previous studies on fluid-structure interaction problems is given in Chapter 2.

The theoretical basis of modal analysis is reviewed in Chapter 3. Some practical considerations related to the experimental modal analysis, such as the B&K 2034 analyzer involved in data acquisition, and STAR software used in modal pararneter estimation are also discussed.

Chapter 4 deals with the experimental study on the CFCF and SFSF plates both in air and in water of 6 different depths of submergence, respectively. A notched plate with clamped ends is suggested to approach the SFSF plate, and finite element software ABAQUS is used to determine the dimensions of the notch. Results and discussion are presented.

An analytical solution to an elastic rectangular plate, which undergoes flexural bending vibration in a body of homogeneous, incompressible and inviscid fluid whose motion is irrotational, is presented in Chapter 5. The relationship between the added mass and the depth of submergence is established. Also, the validity of the presented solution is assessed by applying it to the CFCF and SFSF plates.

Chapter 6 makes conclusions on the study.

Chapter 2

Literature Review

2.1 Previous Work on the Fluid-Structure Interaction Problems

2.1.1 Analytical Approaches

The analytical study on fluid-structure interaction problems was initiated by Rayleigh [1877]. He calculated the increase of inertia for a rigid vibrating plate in an infinite baffle. Afterwards, Lamb[1921] considered the problem for the first axisymmetric flexural mode of a circular plate clamped at its edge. The plate was placed in an aperture of infinitely rigid plane wall in contact with water. The method developed was based on the calculation of the kinetic energy of fluid in terms of the velocity potential; and the Rayleigh method was used in the calculation of the resonance frequency of the plate in fluid. Lamb's work was extended to the case of the vibration of a circular plate by Peake and Thurston[1954], for two different boundary conditions at its edge, simply supported and clamped. Their theoretical results agreed with the experimental data to within 10%.

Kwak and Kim[1991] also investigated the fluid effect on the natural frequencies of circular plates in water. The plate was simply-supported, clamped and free,

respectively, at its edge and underwent axisymmetric vibrations. The Hankel Transformation technique was used to obtain a qualitative measure of the fluid effect. It was found that the natural frequencies of clamped and simply supported circular plates were sensitive to the fluid boundary conditions while the natural frequency of the free edge plate was not sensitive to it.

The approach presented by Espinosa and Gallege-Juarez[1984] is for evaluating the fluid effect on the frequencies of circular plates. Unlike other analyses, no assumption was made as to the magnitude of the wavelength in respect to the linear dimensions of the plate. The method was applied to a water-loaded circular plate vibrating in its axisymmetric modes and confirmed by experiment study.

Dowell and Voss[1963] examined a clamped rectangular plate in contact with fluid and presented a method to estimate the effect of fluid loading on its natural frequencies. It was found that the fluid acted as an aerodynamic spring or as an added mass attached to the plate. Pretlove[1965] extended Dowell and Voss's work considerably. By considering a simply supported plate loaded on one side by a finite fluid-filled cavity, he addressed a problem in reconciling plate and fluid boundary conditions. The plate displacements were expressed as a weighted sum of mode shapes of the plate in vacuo and expanded in terms of orthogonal functions which individually satisfied the fluid boundary conditions. Thus, fluid and plate boundary conditions were satisfied simultaneously. However, the displacement expression is not in terms of normal modes of the combined system, as the mode shapes in vacuum are not eigenfunctions of the coupled governing equation.

More recently, Qaisi[1988] has studied the simply supported and the clamped plates by similar methods. His study extended previous work by the application

of matrix methods to evaluate natural frequencies and mode shapes of the plate in contact with fluid.

Junger and Feit[1972] also considered a simply supported plate. In the analysis, the surface displacement was expanded as a weighted sum of modes of the plate in vacuo, but fluid side wall boundary conditions were not included. The near field and far field responses were discussed. It was concluded that the plate-fluid coupling is small for large plates, in which the only effect of the fluid is as an added mass. Davies[1971] discussed this coupling in some detail, examining the relation to the damping and added mass effects.

The analysis presented by Robinson and Palmer[1990] is of a problem in which the plate and fluid modes are compatible; the plate mode shapes are not coupled by the fluid. Unlike the above analyses, the hydrostatic pressure exerted by the displaced liquid was incorporated. Free motion in a general combined mode was investigated, and constraints on the mode shapes developed. The particular case of a floating plate with edges constrained to have zero slope was then studied.

The above analytical approach has advantages for predicting the effect of the surrounding fluid on the vibrating plates qualitatively, but it is restricted to very special cases. In contrast, numerical approaches such as the finite element method(FEM) and the boundary element method(BEM) make it possible to solve complex structures as well as complex boundary conditions of the structure and fluid.

2.1.2 Numerical Approaches

In the effort to numerically solve the structure-fluid interaction problems, various approximate methods have been proposed to define the transient interaction loading.

They are often based upon the asymptotic behaviours of fluid wave motion, i.e., at early time(high frequency) of the interaction the fluid loading tends to be a damping force and at late time(low frequency) to tends to be an inertia force of added mass.

Everstine[1991] investigated a cylindrical shell with flat end closures submerged in fluid by finite element method and boundary element method. The low frequency vibration was considered, and fully-coupled added mass matrices were calculated. The FEM was implemented using NASTRAN while the BEM was performed using NASHUA and NASTRAN. Both methods were proved capable of computing accurate submerged resonances.

Another rigorous finite element method for fluids was developed and discussed by Chowdhury[1972], which was used by Muthuveerappan[1978, 1979, 1980] to carry out extensive studies on the structure-fluid interaction problems. The study was carried out for a square cantilever plate by varying the following factors: (i) depths of immersion; (ii) aspect ratios; (iii) plate boundary conditions(simply supported, clamped and free at its edges); (iv) plate materials(steel, aluminum and copper); and (v) fluid densities. Results presented indicated the dependence of the natural frequencies of the submerged cantilever plate on depth of water above and below the plate, and on the lateral extent of the water. As the submerged depth increased the variation in natural frequencies became less, and this variation was appreciable only in the fundamental frequencies. The mode shapes in water varied slightly from those in air. Relationships were established showing the dependence of the non-dimensional frequency parameters on plate materials and fluid densities.

Fu and Price[1987] investigated plate-fluid interaction problem by using hydroelasticity theory and being accomplished by the FEM. The plate considered was of can-

tilever support, partially or totally immersed in fluid. The interactions were defined in terms of dry mode shapes, natural frequencies, principal coordinates, frequency-dependent generalized hydrodynamic coefficients, etc.

The effect of the free surface was considered. The validity of the hydroelasticity theory and the accuracy of the chosen numerical techniques were assessed by comparing predictions with the experimental data available.

Numerical methods, whether FEM or BEM, can be applied to solve complex fluid-structure interaction problems. However, both methods require enormous amounts of computational time and effort. Furthermore, it is not easy to obtain an accurate measure of the fluid effects by either method. Besides, the validity of the results obtained by the analytical method or the numerical methods can be appropriately assessed only by experimental study. Thus, experimental methods have been widely used in the investigation of the addressed problems.

2.1.3 Experimental Approaches

Jezequel[1983] carried out a study whose main goal was to obtain an experimental model which could be used in the modal synthesis methods. The added mass was identified by using the measured modes of the structure, both in air and in contact with the fluid. The model which expresses the dynamic behaviour of the fluid-structure system was obtained through an optimization procedure. The method was confirmed by applying it to the case of a plate partially immersed in water.

Randall[1985] carried out dynamic studies on a cylindrical structure in air and submerged in water. Modal analysis techniques were used to identify the natural frequencies and mode shapes under both conditions.

De Santo[1981] accomplished experimental study on perforated plates vibrating in water. The water effect was expressed in terms of added mass and hydrodynamic damping. Dimensionless formulas which gave accurate values for the added mass and lower bounds for the hydrodynamic damping force in the linear and nonlinear damping ranges were presented.

Lindholm et al.[1965] studied extensively cantilever plates in air and in water by experiments. The plates were vertically-placed or tilted, with different aspect ratios, chord ratios and thickness. The results were compared with theoretical predictions based on simple beam theory or thin-plate theory and the chordwise hydrodynamic strip theory. An empirical correction factor was introduced to achieve good theoretical and experimental correlation. The fluid free surface and partial submergence effects were also investigated. It was concluded that: (i) natural frequencies of the plate decreased and node lines of mode shapes shifted when it was submerged in fluid; (ii) the added mass factor changed with the submerged depth of the plate, but the significant change occurred only when the submerged depth was less than about one half span length of the plate.

The experimental studies carried out by Budipriyanto[1993] examined uncracked and cracked cantilevered plates in air and submerged in water. It was found that the natural frequencies reduced by as high as 26.8% and the damping increased by 5 times in-air value when the water level was just about the middle of the plate thickness. For full submergence where the water level was about 230mm above the upper surface of the plate, a maximum natural frequency reduction of 40% and damping increase of about 6 times in-air value were observed.

2.2 Summary

Previous studies which have been reviewed above have investigated the dynamic characteristics of structures in fluid. Most of these studies have examined the change in natural frequencies of the structures due to the presence of the fluid. Some have studied the changes in damping ratios and mode shapes. The mechanism of the fluid-structure interaction problems has been exposed. The study presented in this thesis is focused on the study of the effect of the depth of submergence on the vibration of rectangular plates oriented horizontally. The effect of plate boundary conditions on the vibration of plates submerged in fluid is also investigated. Both analytical and experimental methods are used.

Chapter 3

Modal Analysis Theory

Modal analysis is the process of characterizing vibration properties and behaviour of a linear system by modal parameters. This process is often referred to as modal modelling. Modal modelling focuses on three key properties of a vibrating system: natural frequencies, damping ratios, and mode shapes.

In the subsequent sections, theoretical basis of modal analysis will be reviewed; then experimental modal analysis will be addressed. In the discussion of the experimental method of modal analysis, considerable considerations will be given to some practical problems related to the B&K 2034 analyzer and the STAR software developed by Structural Meas irement Systems, which are used in the analysis of the experimentally obtained frequency response functions and the modal parameter estimation. Also, the calculation of added mass factors from the natural frequencies of a vibrating structure in air and in fluid is discussed.

3.1 Theoretical Basis of Modal Analysis

In order to apply modal analysis to a system, this system is assumed to satisfy the following conditions[Allemang, 1987]:

(i) The system is linear. This implies that the response of the system, due to any combination of forces which applied simultaneously, is equal to the sum of the individual response to each of the forces acting alone. Under this assumption, the system behaviour can be characterized by a controlled experiment, in which forces applied to the system have a form convenient for measurement and parameter estimation rather than being similar to the forces actually applied to the system in its normal environment.

(ii) The system is time-invariant. This means that the system parameters such as the equivalent mass, the stiffness and the damping ratio are constants instead of functions in time.

(iii) The system is considered to follow Betti-Maxwell's reciprocal theorem. The theorem states that the deformation at point j due to a force applied at point k is equal to the deformation at point k due to a force at point j. Under this assumption, it is required to measure only a column or a row of the system frequency response functions.

Consider the governing equation of vibration for a multiple degree-of-freedom system with viscous damping

$$[M]\{\ddot{x}(t)\} + [C]\{\dot{x}(t)\} + [K]\{x(t)\} = \{f(t)\} \tag{3.1}$$

where

$[M]$: $n \times n$ mass matrix;

$[C]$: $n \times n$ damping matrix;

$[K]$: $n \times n$ stiffness matrix;

$\{\ddot{x}(t)\}$: $n \times 1$ vector of accelerations;

$\{\dot{x}(t)\}$: $n \times 1$ vector of velocities;

$\{x(t)\}$: $n \times 1$ vector of displacements;

$\{f(t)\}$: $n \times 1$ vector of forces.

Application of Laplace transform to Equation 3.1 yields

$$[s^2[M] + s[C] + [K]]\{X(s)\} = \{F(s)\} + ([M] + [C])\{X(0)\} + [M]\{\dot{X}(0)\} \quad (3.2)$$

where $s = \delta + jw$ is the Laplace variable; $\{X(0)\}$ and $\{\dot{X}(0)\}$ are the initial displacement and velocity vectors at time t = 0; $\{X(s)\}$ and $\{F(s)\}$ are the displacement and force vectors in the Laplace domain. If the initial conditions are zero, Equation 3.2 becomes

$$[s^2[M] + s[C] + [K]]\{X(s)\} = \{F(s)\} \quad (3.3)$$

Let $[B(s)] = s^2[M] + s[C] + [K]$, then Equation 3.3 can be rewritten as

$$[B(s)]\{X(s)\} = \{F(s)\} \quad (3.4)$$

This is an equivalent representation of Equation 3.1 in the Laplace domain. By defining $[H(s)] = [B(s)]^{-1}$, Equation 3.4 becomes

$$\{X(s)\} = [H(s)]\{F(s)\} \quad (3.5)$$

where $[H(s)]$ is called the transfer function matrix. Let the Laplace variable $s = j\omega$, then one has

$$[H(j\omega)] = [B(j\omega)]^{-1} = \frac{adj[B(j\omega)]}{det[B(j\omega)]} \quad (3.6)$$

where $[B(j\omega)] = [-[M]\omega^2 + j\omega[C] + [K]]$; $adj[B(j\omega)]$ is the adjoint matrix of $[B(j\omega)]$ and $det[B(j\omega)]$ is the determinant of $[B(j\omega)]$.

Since both the adjoint matrix of $B[(j\omega)]$ and the determinant of $[B(j\omega)]$ are polynomials in $j\omega$, the element of $[H(j\omega)]$ is a rational fraction in jw. Therefore, it is possible to represent any element of the frequency response function matrix $[H(j\omega)]$ in a partial fraction form:

$$[H(j\omega)] = \sum_{r=1}^{n} [\frac{[A_r]}{j\omega - \omega_r} + \frac{[A_r^*]}{j\omega - \omega_r^*}] \tag{3.7}$$

where $[A_r]$ is the r-th residual matrix which reflects the corresponding mode shape; ω_r is the r-th complex frequency, whose imaginary part gives the damped natural frequency and whose real part gives the damping coefficient. A * designates the corresponding complex conjugate.

For the homogeneous solution:

$$[B(j\omega)]\{X(j\omega)\} = \{0\} \tag{3.8}$$

The characteristic polynomial equation is obtained from

$$det[B(j\omega)] = 0 \tag{3.9}$$

The roots ω_i of the characteristic Equation 3.9 are called eigenvalues or complex frequencies. Substituting an eigenvalue into the equation of motion 3.8, solving for $X(j\omega)$ and normalizing the values of $X(j\omega)$ to unity yield the eigenvector U_i corresponding to the eigenvalue ω_i.

It can be shown that modal vectors are orthogonal with respect to one another if they are weighted with respect to the mass matrix [M] and the stiffness matrix [K]. It can also be shown that modal vectors are orthogonal to one another if they are weighted with respect to the damping matrix [C] when proportional damping is assumed.

Equation 3.1 can be written in the modal space. The transformation from physical space to modal space is given by

$$\{x(t)\} = [U]\{q(t)\} \tag{3.10}$$

where

$[U]$: modal matrix, $[U] = [U_1, U_2, \ldots, U_n]$;

{q(t)}: displacement vector in modal space.

Substitution of Equation 3.10 into Equation 3.1 gives

$$[M][U]\{\ddot{q}(t)\} + [C][U]\{\dot{q}(t)\} + [K][U]\{q(t)\} = \{f(t)\} \tag{3.11}$$

Pre-multiplying by $[U]^T$ gives

$$[U]^T[M][U]\{\ddot{q}(t)\} + [U]^T[C][U]\{\dot{q}(t)\} + [U]^T[K][U]\{q(t)\} = [U]^T\{f(t)\} \tag{3.12}$$

When the damping of the system is proportional, application of the orthogonality properties of modal vectors yields the generalized diagonal mass, stiffness and damping matrices:

$$[\overline{M}] = [U]^T[M][U] \tag{3.13}$$

$$[\overline{C}] = [U]^T[C][U] \tag{3.14}$$

$$[\overline{K}] = [U]^T[K][U] \tag{3.15}$$

Rewriting Equation 3.12 as

$$[\overline{M}]\{\ddot{q}(t)\} + [\overline{C}]\{\dot{q}(t)\} + [\overline{K}]\{q(t)\} = \{P(t)\} \tag{3.16}$$

where $\{P(t)\} = [U]^T\{f(t)\}$ is the force vector in modal space. It is noticed that each equation uncouples from the other and represents an individual modal response of the system[Ewins, 1984].

3.2 Experimental Modal Analysis

Experimental modal analysis is the process of experimentally determining the modal parameters of a linear, time-invariant system. Equation 3.7 is the general matrix form that is used in modal analysis. Continuous systems have an infinite number of degree-of-freedom; however, in general, only a finite number of modes are needed to describe the dynamic behaviour of a system. In the frequency range of interest, the modal parameters can be estimated to be consistent with Equation 3.7. In the lower and higher frequency ranges, residual terms can be included to handle modes in these ranges. In this case, Equation 3.7 becomes

$$H_{ik}(j\omega) = P_{ik}(j\omega) + \sum_{r=1}^{n}[\frac{A_{ikr}}{j\omega - \omega_r} + \frac{A^*_{ikr}}{j\omega - \omega^*_r}] + Q_{ik}(j\omega) \tag{3.17}$$

where $P_{ik}(j\omega)$ is lower residual, and $Q_{ik}(j\omega)$ upper residual. In many cases the lower residual is called the residual inertia which reflects the inertia of the lower modes and is an inverse function of the frequency squared; and the upper residual is called the residual flexibility which reflects the flexibility of the upper modes and is constant with frequency.

In experimental modal analysis, frequency response functions are used as inputs so that modal parameters could be estimated. Since it is assumed that the Betti-Maxwell theorem can be applied to the system, modal parameters can be estimated by measuring either a column or a row of the system frequency response functions. Thus, the frequency response function plays an important role in the experimental modal analysis. The frequency response functions are firstly determined by experiments and then used to estimate the natural frequencies, modal damping ratio, and mode shapes of the system. Thus the experimental modal analysis comprises mainly of two

phases, the measurement of frequency response functions and the modal parameter estimation.

3.2.1 Measurement of Frequency Response Functions

Before discussing the measurement of frequency response functions, an appropriate excitation signal should be chosen.

Excitations which are widely used to drive the tested structure in order to measure frequency response functions include slow-sine sweep, fast-sine sweep, impact(impulse), step relaxation, and random. The fast-sine sweep was used to drive the plates in this experimental study. The advantages of using the fast-sine sweep are: the relatively short measurement time, the possibility of reducing leakage error and the high signal to noise ratio[Ewins, 1984].

The fast-sweep sine is a periodic deterministic signal. It is formulated by sweeping a sine wave signal up and down within a frequency band of interest during a single sample period. The suitability of the sweep rate can be checked by trial and error. Measurement is made twice by once sweeping up and the second time sweeping down through the frequency range. If the same curve results in the two cases, then the sweep rate is appropriate.

In this experimental study, the B&K 2034 analyzer is chosen to take the measurement of frequency response functions. It is a fast, flexible, and fully self-contained two-channel Fast Fourier Transform analysis system. The resolution lines are 801.

Noise will be unavoidably involved in the measurement. This noise can result from three sources: (i) noncoherent noise resulting from stray electrical signals or unmeasured excitation sources; (ii) signal processing noise produced during analysis

due to the use of discrete Fourier Transform to convert time into frequency domain or vice versa; and (iii) nonlinear noise due to non-linear behaviours of the studied system needed to be considered in the signal processing methods. These noises are eliminated by utilizing a signal averaging procedure and sufficient length of data with proper windows and frequency resolution.

The B&K 2034 analyzer provides five error reduction techniques to minimize errors in the measurement of frequency response functions: (i) choice of the appropriate frequency response function estimator; (ii) use of signal averaging methods; (iii) choice of proper frequency resolution, and (iv) use of a suitable weighting function or window. Appropriate consideration should be given to each of these in order to ensure that 'correct' measurement is made.

Frequency Response Function Estimator

Based on the assumed noise input into the system, the frequency response function estimating procedure can be grouped into three different methods, i.e., H_1, H_2 and H_v. H_1 assumes that noise exists in the output and the input is free of noise. Hence

$$[H_1]\{X\} = \{Y\} - \{\eta\} \tag{3.18}$$

H_2 assumes that the noise is present in the input and absent in the output,

$$[H_2]\{\{X\} - \{\xi\}\} = \{Y\} \tag{3.19}$$

H_v assumes the noise to exist both in the input and output signals, consequently

$$[H_v]\{\{X\} - \{\xi\}\} = \{Y\} - \{\eta\} \tag{3.20}$$

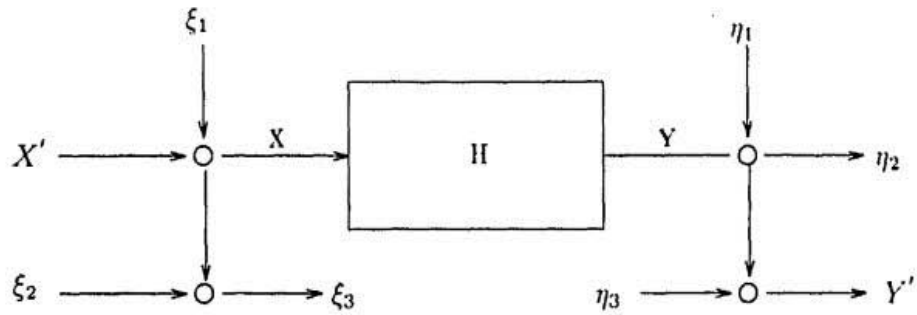

Figure 3.1: A system with noise

The B&K 2034 analyzer utilizes the spectral approach for estimating frequency response functions given by[B&K 2034 analyzer manual, 1987]

$$H_1 = \frac{G_{xy}}{G_{xx}} \tag{3.21}$$

$$H_2 = \frac{G_{yy}}{G_{yx}} \tag{3.22}$$

where

G_{xx} is the input auto-spectrum and equal to $\sum_{i=1}^{n} X_i X_i^*$;

G_{yy} is the output auto-spectrum and equal to $\sum_{i=1}^{n} Y_i Y_i^*$;

$G_{xy} = G_{yx}$ is the cross-spectrum, and equal to $\sum_{i=1}^{n} X_i Y_i^* = \sum_{i=1}^{n} Y_i X_i^*$.

In an actual measurement situation, the noise occurs both in the input and output as shown in Figure 3.1 in which apostrophe denotes the true measured input and output. Therefore, H_1 and H_2 are further defined as

$$H_1 = \frac{H}{1 + c_1}$$

$$H_2 = H(1 + c_2)$$

where

H is the true frequency response function of the system;

$\epsilon_1 = \frac{G_{\xi\xi}}{G_{xx}}$ is the relative amount of noise at the input, $\xi = \xi_1 + \xi_2$;

$\epsilon_2 = \frac{G_{\eta\eta}}{D_{yy}}$ is the relative amount of noise at the output, $\eta = \eta_1 + \eta_2$.

It can be seen that H_1 is the lower bound and H_2 is the upper bound of H.

The level of confidence in frequency response function measurement can be estimated by the coherence function which is defined as

$$\gamma^2 = \frac{|G_{yx}|^2}{G_{xx}G_{yy}} = \frac{G_{xy}G_{yx}}{G_{xx}G_{yy}}$$

γ^2 is real valued and varies from 0 to 1. Zero value of the coherence function means that the response is generated by noise or a source other than measured input. When the coherence function is one, however, the measurement is perfect, i.e., the output is caused by the measured input.

Leakage And Windowing

Leakage is a direct consequence of the truncation which occurs during sampling a finite length of time history coupled with the assumption of periodicity. One practical solution to the leakage problem involves the use of weighting functions or windows. Windowing involves the imposition of a prescribed profile on the time signal prior to performing the Fourier Transform. By applying a weighting function or a window, error in frequency response functions can be reduced.

Windows available in the analyzer are Rectangular, Transient, Exponential, Hanning, Flat Top and Kaiser Bessel[B&K 2034 analyzer manual, 1987]. Allemang[1987] suggests the use of Hanning window for stationary signals. In this study, Hanning window is used in the signal analysis.

Averaging

Signal averaging is the process involving several individual time records, or samples, before a result, which can be used with confidence, is obtained. Error caused by leakage and spurious random noise can be reduced by averaging so that the accuracy and statistical reliability of frequency response functions are improved.

Several time averaging methods, such as Linear, Exponential and Peak Averaging, are available in the analyzer. These can be performed with or without the overlapping of the time record. The overlap process in intended to enhance the measured data by including consecutive history data before the previous data are completed. In the analyzer, the degree of overlap could be 50%, 75% or a maximum of 85%. The number of averaging required are determined by two major considerations, the accuracy and statistical reliability desired, and the noise level in signals. In the experiment of this study, Linear Averaging method with 75% overlap was used and the number of averaging was 20.

Zoom

Because of the constraints imposed by the limited number of discrete points available due to the block size, the maximum frequency range to be covered and/or the length of time sample available or necessary to provide good data, the limitations of inadequate frequency resolution arise. The common solution is to 'zoom' in the frequency range of interest and to concentrate all the spectra lines into a narrow band between f_{min} and f_{max}.

In addition, increase of the frequency resolution minimizes the leakage error. Zoom means the reduction in frequency span of measurement which automatically

requires a longer time history record. When the frequency response function peak is narrower than the frequency resolution, error occurs. In this case the frequency response function will "leak" or be wider than the region of interest. Resonant and anti-resonant peaks of the frequency response function are susceptible to this type of error. In the experiment carried out in this study, zoom of 50Hz frequency span is used to obtain more accurate measurement.

3.2.2 Modal Parameter Estimation

Modal parameter estimation is the estimation of frequency, damping, and mode shape from the measured data which may be (i) in a relatively raw form in terms of force and response data in the time or frequency domain or (ii) in a processed form such as frequency response or impulse-response functions. Modal parameter estimation carried out in this study is based upon the measured data being the frequency response functions. The computer software package used to perform the estimation is STAR(Structural Testing, Analysis and Reporting), version 4.00, developed by Structural Measurement Systems. Besides its capability to identify the modal properties of mechanical structures, STAR provides functions such as measurement display, real-time animated mode shape display and data handling.

When a structure is excited using a broadband input force, many modes of vibration are excited simultaneously. Since the structure is assumed to be linear, frequency response functions are really made up of the sums of the resonance curves for each vibration mode. In other words, at any given frequency, the frequency response function is made up of the sum of motions of all the modes of vibration which have been excited. However, the contribution of each particular mode to the

overall motion is generally greatest in the vicinity of its resonance peaks.

The amount of the contribution due to adjacent modal resonance curves to the overall frequency response function value at a mode's natural frequency is called modal coupling. The degree of modal coupling in a frequency response function is governed by the modal damping ratio and the frequency separation of the modes. According to the mode-coupling degree of a system, two modal parameter estimation techniques, (i) single degree-of-freedom(SDOF) approximations and (ii) multiple degree-of-freedom(MDOF) approximations, can be used. These two techniques are available in STAR[STAR manual, 1990].

SDOF Techniques

In cases where modal coupling is light, the frequency response function data in the vicinity of each modal resonance peak can be treated as if they are the responses of a SDOF system or a single mode of vibration. In other words, in the measurement of frequency response functions of a system with light modal coupling, it is assumed that the contribution of the tails of adjacent modes near each modal resonance peak is negligible. Algebraically, this means that the magnitude of the frequency response function is effectively controlled by one of the terms in the series, that being the one relating to the mode whose resonance is being observed. In this case, SDOF curve fitting methods can be used to identify the modal parameters.

STAR provides several SDOF techniques, such as Coincident Peak, Quadrature Peak, Complex Peak and Polynomial. When using a SDOF technique, modes in the test data should be relatively uncoupled. A peak on an frequency response function plot should occur in relative isolation from other peaks and should be relatively

uncontaminated by residual contributions from higher and lower modes. One key disadvantage is that they tend to be less accurate than the more sophisticated MDOF techniques. If accuracy is not a top priority, SDOF techniques can provide results with minimum effort and computer resources.

MDOF Techniques

where modal coupling is heavy, an SDOF modal parameter estimation method may yield parameters with large errors. In cases of heavy modal coupling, the parameters of all the modes must be estimated simultaneously using a MDOF method. STAR provides users with a MDOF estimation technique named the Rational Fraction Least Squares(RFLS) polynomial method. This method fits a polynomial function in a rational fraction form, to a frequency response function using a least square error technique.

The RFLS method allows users to have better chance of accurately determining how many modes are actually in the specified frequency range. This is accomplished by over-specifying the maximum number of modes. There may be repeated modes, or modes very close in frequency, that appear as one mode. By over-specifying the maximum number of expected modes, one has better chance of accurately determining mode size in the specified frequency range. The true(actual) modes and computational(artificial) modes of the structure are identified according to the "Stability Diagram" window[STAR manual, 1992]. As stated earlier, MDOF estimation techniques offer improved accuracy in cases where the frequency response function data contain heavy modal coupling and/or the structure has local modes. However, they are more demanding of computer resources.

3.3 Added Mass Factors

When a structure is submerged in fluid, natural frequencies decrease and damping ratios increase. It is more appropriate to use the non-dimensional value, added mass factor(AMF), to measure the change in natural frequencies due to the fluid-loading effect. The added mass factor to be determined is based on the obtained modal parameters. The necessary parameters are natural frequencies of tested structures in vacuum and in fluid. For structures having a relatively higher density, the natural frequency in air is sufficiently close to the that in vacuum. This allows the use of the in-air natural frequency for added mass calculations.

For continuous systems such as plates, the systems have an infinite number of degrees-of-freedom. However, in general, only a finite number of modes are needed to describe the dynamic behaviour of a system. As stated earlier, modal parameters of these modes can be estimated from the measured frequency response functions in the frequency range of interest. Also, because of the orthogonality of mass, stiffness and damping matrices with respect to the mode shape matrix, the dynamic characteristics of the system can be represented as, in modal space,

$$\overline{M}_i\ddot{q}_i + \overline{C}_i\dot{q}_i + \overline{K}_iq_i = 0 \quad i = 1, \ldots, n \tag{3.23}$$

where $\overline{M}_i$, $\overline{C}_i$ and $\overline{K}_i$ are the modal mass, modal damping and modal stiffness of the i-th mode, respectively. The undamped natural frequency is

$$\omega_i = \sqrt{\frac{\overline{K}_i}{\overline{M}_i}} \tag{3.24}$$

When a structure vibrates in fluid, it is subject to fluid effect. As stated earlier, the fluid effect can be accounted for by an added mass and added damping ratio. From

this point of view, Equation 3.24 is valid for a vibrating plate both in air and in fluid. Also, because physical stiffness of the plate remains unchanged whether it is in air or in fluid, modal stiffness $\overline{K}_i$ remains the same if mode shapes are assumed unchanged due to the presence of fluid. In this case, one has

$$\frac{\overline{M}_{ifluid}}{\overline{M}_{iair}} = \frac{\omega_{iair}^2}{\omega_{ifluid}^2} \tag{3.25}$$

where $\overline{M}_{iair}$ and $\overline{M}_{ifluid}$ are the modal masses of the i-th mode of the structure in air and in water, respectively. If M_i^* is used to designate the added mass due to the fluid effect on the structure, then $\overline{M}_{ifluid}$ can be written as

$$\overline{M}_{ifluid} = \overline{M}_{iair} + M_i^*$$

We define an added mass factor as

$$AMF = \frac{M_i^*}{\overline{M}_{iair}}$$

then from Equation 3.25, one has

$$AMF = (\frac{\omega_{iair}}{\omega_{ifluid}})^2 - 1 = (\frac{f_{iair}}{f_{ifluid}})^2 - 1 \tag{3.26}$$

3.4 Summary

In this chapter, the theoretical basis of modal analysis is reviewed, and experimental modal analysis techniques have been discussed. Some practical problems related to the measurement of frequency response functions and modal parameter estimation have been considered also. In addition, the calculation of added mass factors from the natural frequencies of a vibrating structure in air and in fluid is discussed.

Chapter 4

Experimental Investigation

Experimental studies are an important tool in the investigation of the behaviour of vibrating structures submerged in fluid. Experimental studies make it possible to gain a direct insight into problems whose analytical solution is difficult to obtain.

In this chapter we describe experiments to study the vibration response of two flat plates which are horizontally oriented and with different boundary conditions. Experiments on the plates in air and submerged in water are reported. One of the plates has clamped-free-clamped-free(CFCF) supports while the other has simple-free-simple-free(SFSF) supports. The effect of the depth of submersion on the vibration response has been studied by varing the depth from 0 to 327.5 mm in five steps.

In the subsequent sections, experimental setup used in the study followed by method of calibration are introduced. Detailed study on modelling of the simple supports involved in the boundary conditions of the SFSF plate using finite element software ABAQUS is presented. Description of the modal testings on CFCF and SFSF plates both in air and in the submersion of six different water levels is given. Results and discussion are presented.

4.1 Experiment Setup

To measure the vibration of each plate, 15 PCB 330A accelerometers are used and mounted at acquisition points on the plate. These accelerometers are selected not only because they are light, each weighting 3 grams together with its mounting socket, and as small as $\phi 11 \times 21.5$ mm, but also because they have high sensitivity of 200 ∓ 40 mV/g.

The experiment setup used in the experiment is shown in Figure 4.1. Fast sine sweep excitation was selected so that the best results for coherence and frequency response functions would be obtained. A sweep sine signal generated by the function generator was amplified by a power amplifier then input to the vibration exciter to excite the tested plate through a connecting rod shown in Figure 4.2. A force transducer was attached between the connecting rod and the tested plate to measure the excitation force which then was amplified by the dual mode amplifier. The response signal of the vibrating plate was measured by accelerometers, then amplified by the differential amplifier. Finally, both force and response signals were input to the oscilloscope to monitor and the analyzer to perform Fast Fourier Transform so that frequency response functions and coherence functions were obtained. These data were then exported and stored in a PC computer for analysis using STAR.

The connecting rod between the vibration exciter and the force transducer is comprised of three parts, as shown in Figure 4.2. Part 1 has two functions. One is to connect the vibration exciter to the long steel rod part 2; another is to adapt preload by adjusting the coupling length with part 2. Part 3 is designed to protect instruments from overloading; the middle part whose diameter is $\phi \frac{1}{16}"$ is made of mild steels and will be yielded when the exciting force becomes large.

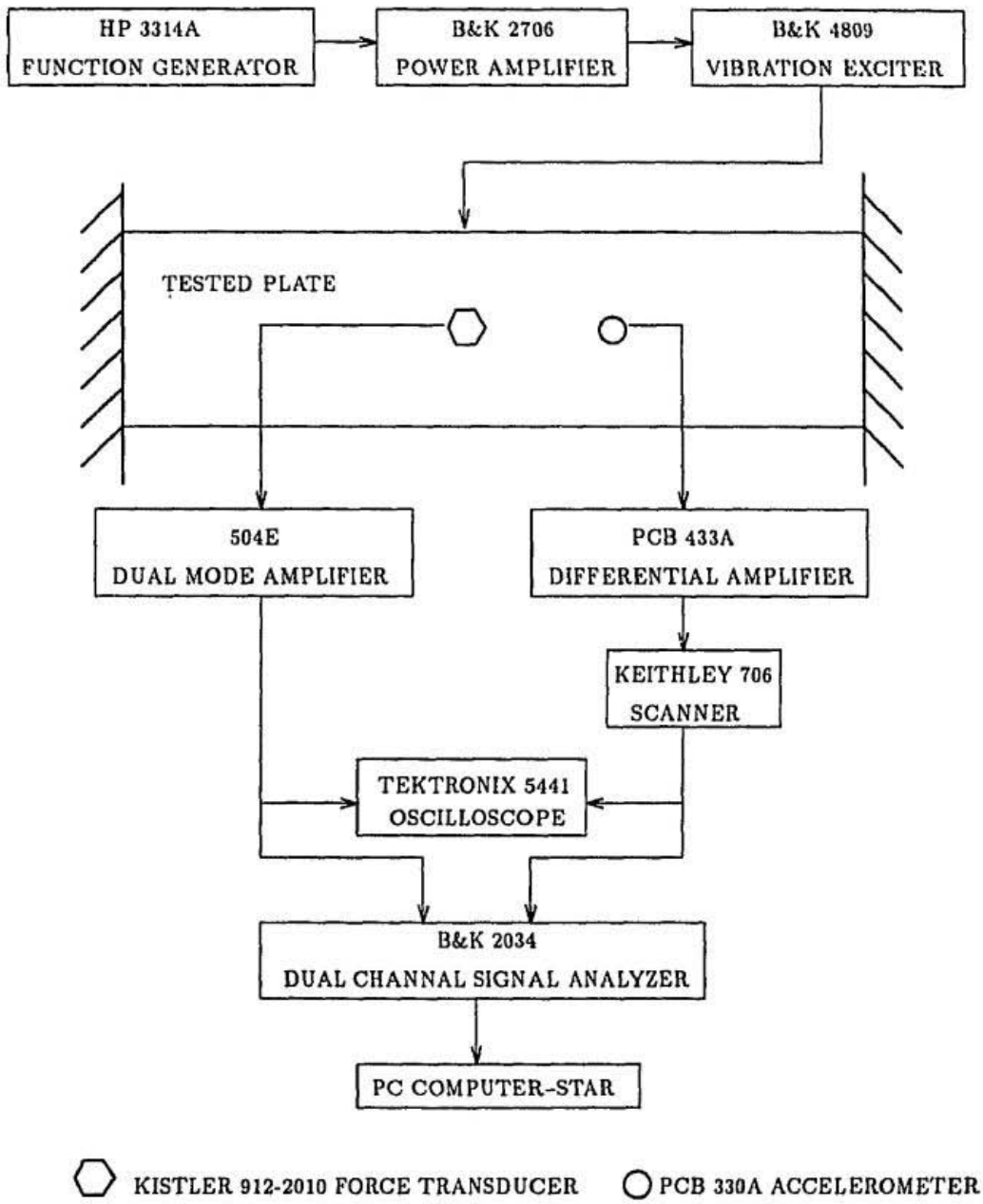

Figure 4.1: Experiment setup

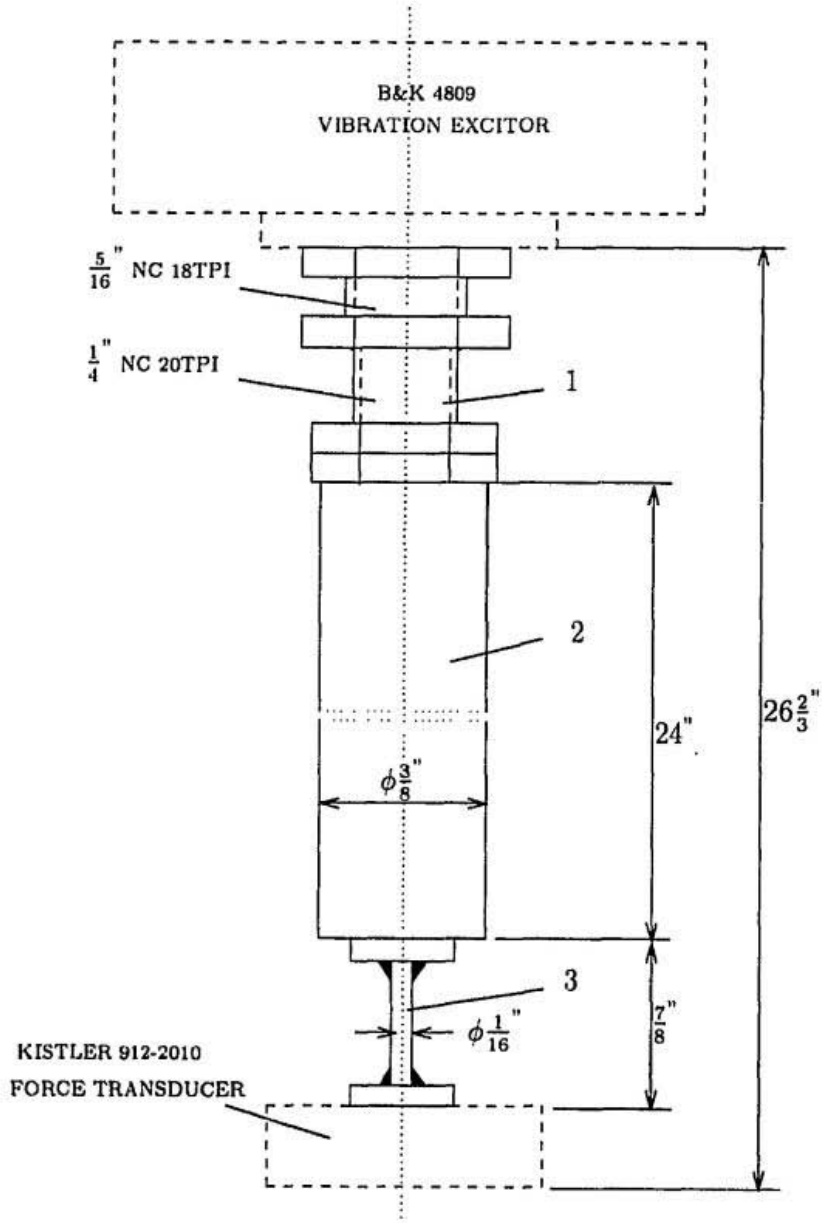

Figure 4.2: Connecting rod

To carry out the measurements in water, a $1300 \times 550 \times 800$ mm tank was built. The wall of the water tank was made of transparent plastics and constructed on steel frames which were used to strengthen the wall. The level of the free water surface with respect to the plate was controlled by the depth of water in the tank. The tank was fixed to a rigid platform so that it did not vibrate when the plate was excited. When the experiment in water was carried out, the accelerometers and all connections of wires submerged in water were water-tight using vaseline. A photograph of the setup is shown in Figure 4.3.

4.2 Calibration

The calibration of the testing system is carried out in two steps. The first step involves the calibration of the excitation channel which includes the force transducer and the dual mode amplifier. The second step involves the calibration of the response channel which includes the accelerometers, the differential amplifier and the scanner.

4.2.1 Excitation Channel

The setup for the calibration is shown in Figure 4.4. The standard weight was applied on the force transducer. The signal produced by the transducer was amplified by the dual mode amplifier which was properly set so that the expected channel sensitivity of 2V/lb was obtained. The multimeter was used to measure the output.

In order to apply the weight on the force transducer, two pieces of $98 \times 74 \times 10$ mm aluminum plates were used. The force transducer was attached to the plates by screws, and the effect from the weight of the plate and screws was avoided by grounding the amplifier before the standard weight was applied. The calibration was

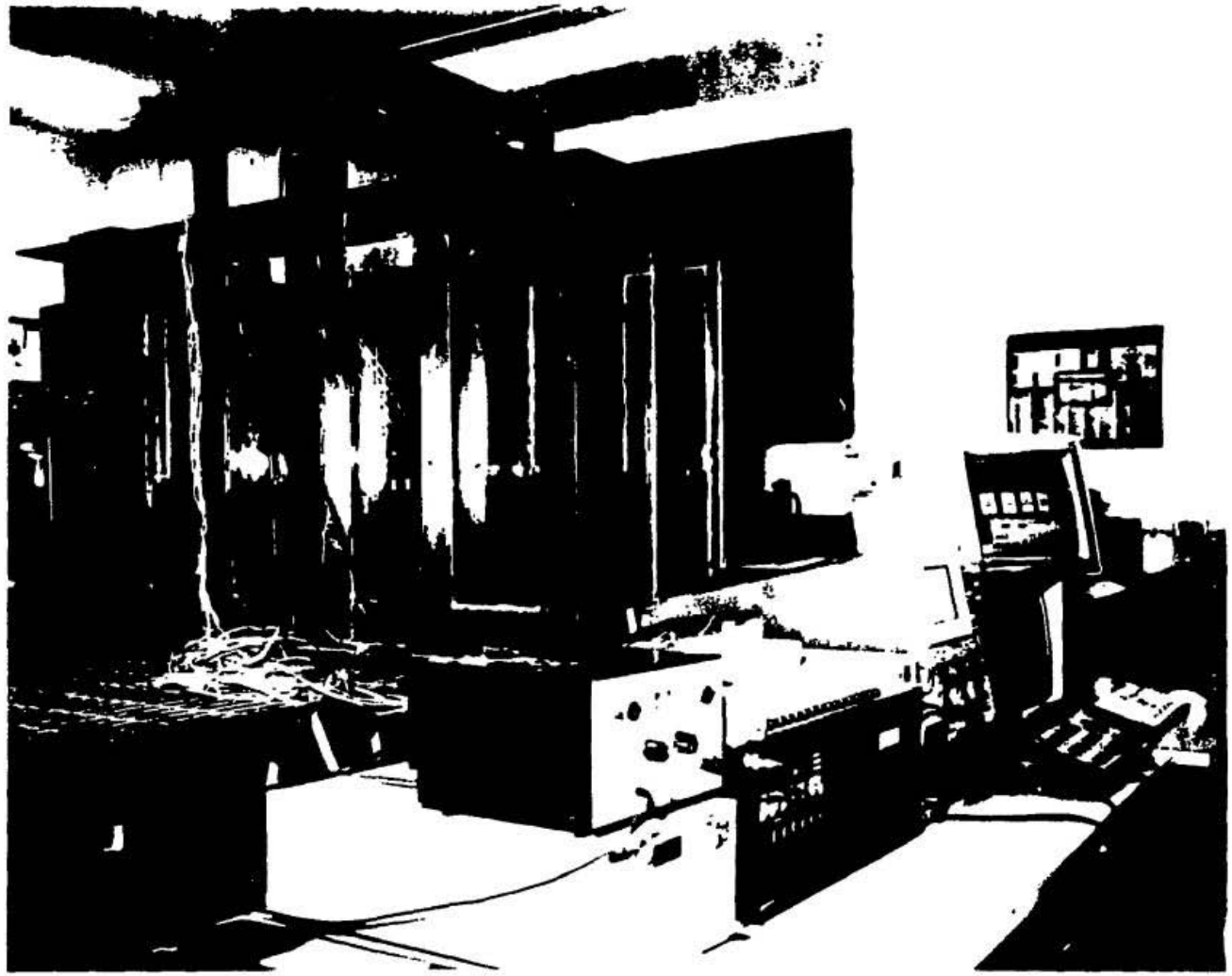

Figure 4.3: Photograph of the setup

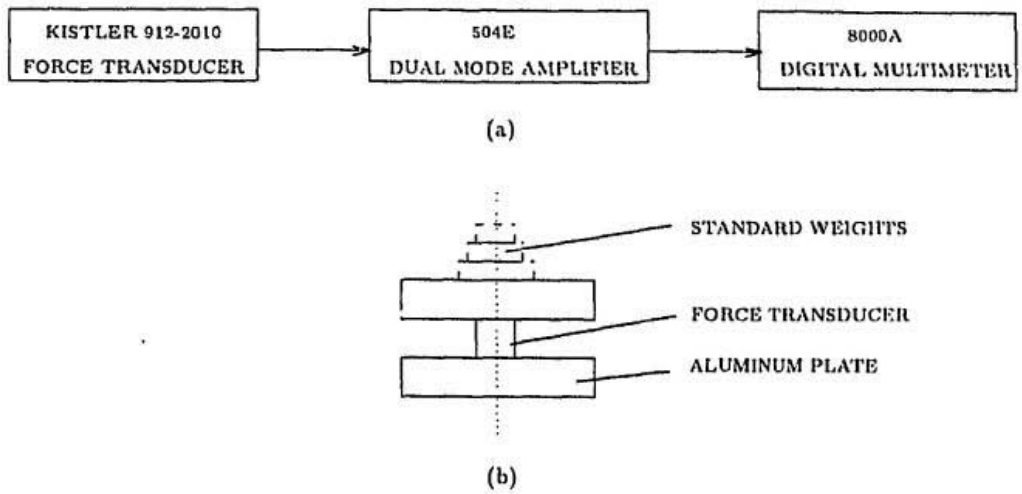

Figure 4.4: (a)Calibration setup for the excitation channel; (b) Setup used to apply loads to the force transducer

repeated five times and the readings were shown in Table 4.1. The sensitivity equation was estimated using the Least Square Method. As expected, the function of the input and the output is linear in the calibration range, which is expressed by

$$y = 0.021428 + 2.118572x$$

Where x is a load in pounds and y is a reading in voltages.

4.2.2 Response Channel

The setup for the response calibration is shown in Figure 4.5. The accelerometer to be calibrated was attached to the socket of the calibrator, which outputs a constant level of 1g(RMS) at a frequency of 80.125Hz. The output of the accelerometer was amplified by the differential power amplifier and sent to the analyzer to calculate the auto spectrum. The sampling time was 8s, averaging number was 20 and Hanning

Table 4.1: The readings of calibration for the excitation channel

Load(lb)	*Reading(V)*				
	1	2	3	4	5
0.5	1.050	1.10	1.08	1.08	1.015
1.0	2.15	2.14	2.16	2.09	2.05
1.5	3.05	3.03	3.02	2.98	3.06
2.0	4.10	4.12	3.99	4.15	4.03
2.5	5.15	5.10	5.08	5.10	5.06
3.0	6.13	6.03	6.04	5.98	6.02
3.5	7.10	6.95	7.00	7.10	7.04
4.0	8.12	8.09	8.14	7.96	8.02
4.5	9.05	9.07	9.01	9.00	9.12
5.0	10.10	10.12	10.10	10.05	10.00

window was used. The calibration for each channel was done one by one, and the scaled sensitivity factor of each channel was then estimated and shown in Table 4.2.

4.3 Tested Plates

The sample length of tested plates is measured 655 × 201.65 × 9.36 mm, which were cut from AISI C-1020 cold-rolled steel plate stock. In order to exclude the effect of material difference between plates, only one plate is used for the two different boundary conditions. One is CFCF supported, another is SFSF supported, which are shown in Figure 4.6. Only the first five modes are of interest.

4.3.1 CFCF Plate

In the experiment, the plate was clamped horizontally between two 300 × 300 × 27.5 mm steel blocks over a plate length of 300mm at each chordwise end. The lower

Table 4.2: The sensitivity factor of the response channels

Channel No.	*Accelerometer series No.*	†*RMS(V)*	*Scaled factor*
1	20502	1.1533	1.3873
2	19912	1.2570	1.2729
3	20093	1.1832	1.3523
4	19944	1.6000	1.0000
5	20397	1.1662	1.3720
6	19593	1.2369	1.2936
7	20082	1.4849	1.0775
8	20505	1.3360	1.1976
9	20403	1.2570	1.2729
10	20236	1.5652	1.0222
11	19579	1.4492	1.1041
12	19612	1.3620	1.1747
13	19906	1.3454	1.1892
14	19907	1.4306	1.1184
15	19568	1.2884	1.2419

† RMS is the Root of Mean Square.

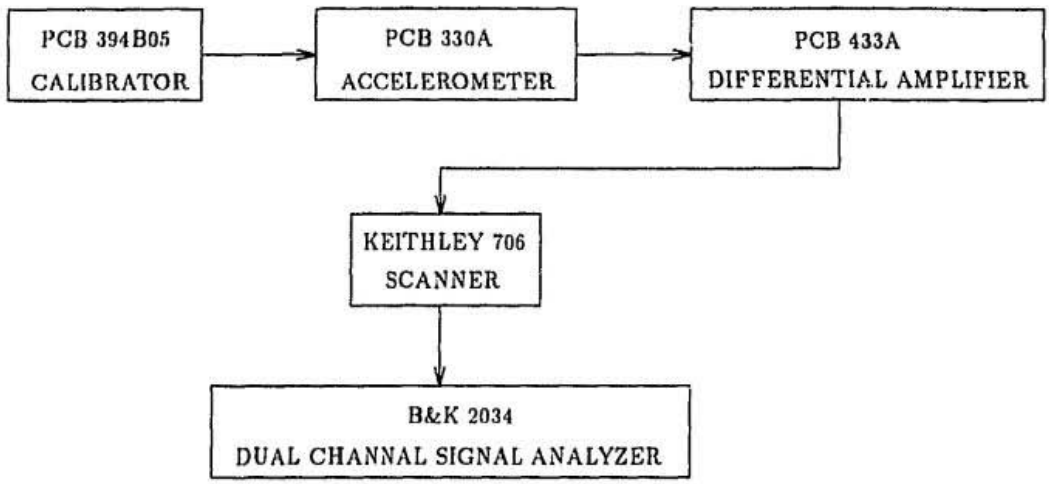

Figure 4.5: Calibration setup for the response channel

block was attached to a heavy I beam support, which was welded to the bottom of the tank. The support height is 275 mm.

4.3.2 SFSF Plate

It is more complicated to obtain the SFSF plate in practice than the CFCF plate. Thus some detailed discussions are called for.

Survey of Different Approaches to A Simple Support

"Hinged" support and "edge" support are widely used to accomplish a simple support. However, a hinge always involves some friction. Thus the moment at a "hinged" support will not be equal to zero. The friction moment may be a constant or proportional to the reaction exerted by the support. For an edge support, then, since the support is off-center, rotation will result in a tangential friction force which produces

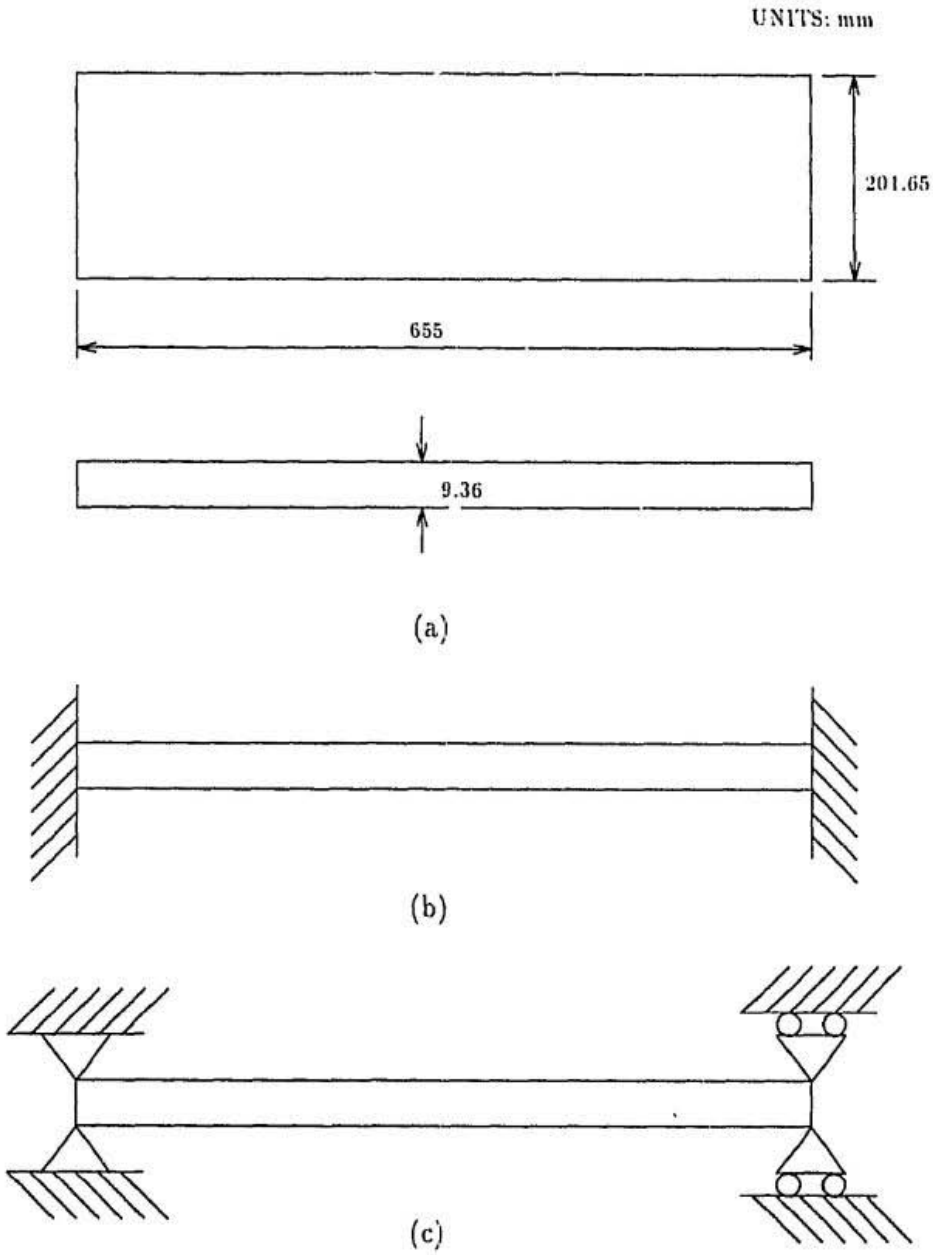

Figure 4.6: (a) Dimensions of the plates; (b)Clamped-free-clamped-free(CFCF) plate; (c)Simple-free-simple-free(SFSF) plate

both a resisting moment and an axial load.

The effect of friction moments at simple supports is similar to that of decreasing the dimensions of a plate, by an amount ranging from close to zero for"frictionless" hinges to a maximum of about one half the thickness. For supports at the two ends, the amount is one times the thickness[Donnell, 1976].

Because of the shortcomings involved in these two approaches, a "notched" plate with a clamped end is suggested to approach the condition of simple supports. Thus, a plate having notches is clamped at the immediate outward ends, as shown in Figure 4.7, can be used to simulate the SFSF plate. Obviously, it is the dimensions of the notches that govern the accuracy of the approach.

Dimensions of the Notch

The finite element method is a powerful tool to predict the dynamic behaviour of systems. In this study, the general purpose finite element program ABAQUS, version 5.1, developed by Hibbitt, Karlsson and Sorensen Inc., was used to determine the optimal dimensions of the notch.

S8R5 shell element was chosen to discretize the plate in this study. It is a 8-node doubly curved shell element; each node has 5 degrees-of-freedom(three displacements and two in-surface rotations). It has a 3×3 middle surface integration for mass, body forces and surface pressure calculation and a 2×2 reduced integration for constitutive calculation and output. 5 integration points are chosen through the shell thickness. They are located from the bottom to the top surface of the shell, with equal distances between two adjacent points[ABAQUS manual, 1992].

In order to select an appropriate mesh for the plate, tentative calculations are

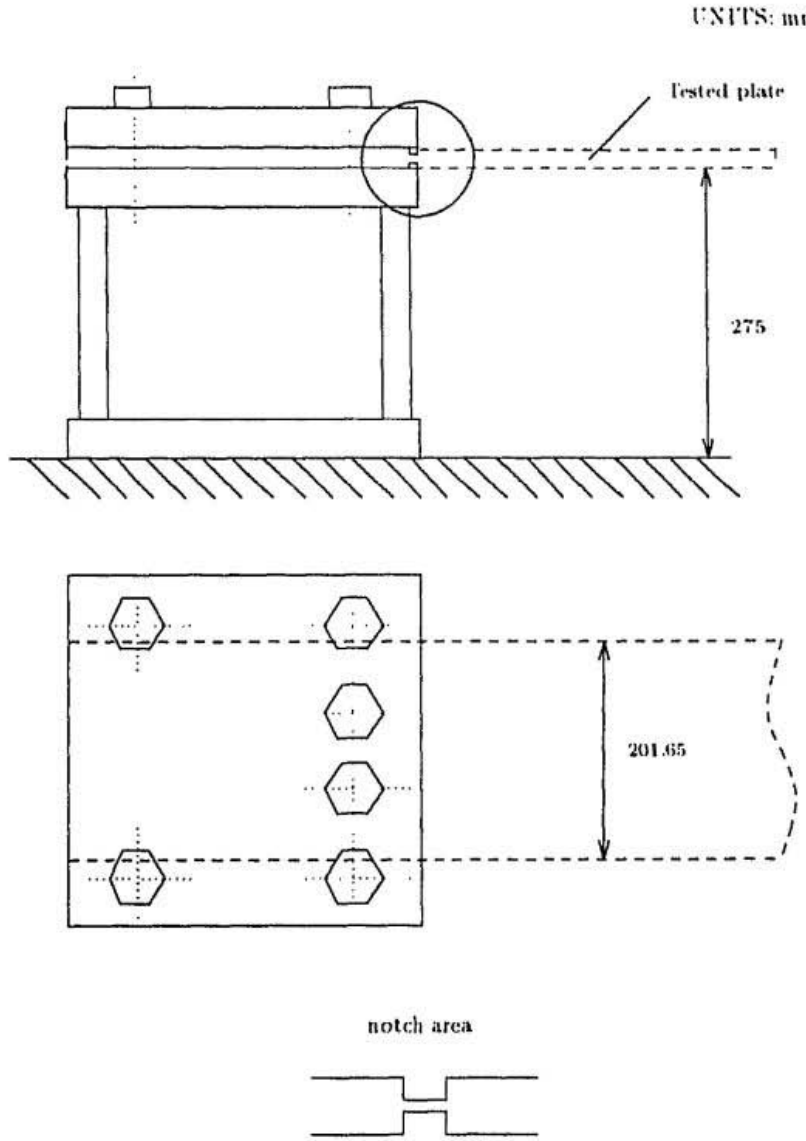

Figure 4.7: Notched plate with a clamped end

Table 4.3: Natural frequencies(Hz) obtained using two meshes

Mode No.	*Mesh 1*	*Mesh 2*
1	51.33	51.33
2	204.01	203.98
3	222.58	221.22
4	459.47	459.39
5	478.55	476.40

performed to a notched plate with notches measured 3×0.6552 mm. Two different meshes are used; mesh 1 has 175 elements, but the size of element changes abruptly; mesh 2 has 413 elements and the size of element changes gradually, as shown in Figure 4.8. The first five natural frequencies of the simulated SFSF plate are calculated and listed in Table 4.3. The results obtained with two meshes correlate quite well between themselves, suggesting that mesh 1 is reasonable and reliable to perform the calculation of the notched plate.

To investigate the effect of the notch dimensions on boundary condition, three notches are investigated. The notches have the width of 3 mm,4 mm and 5 mm which are approximately $\frac{1}{3}h$, $\frac{2}{5}h$ and $\frac{1}{2}h$, respectively. The depth of the notches is measured 0.07h, 0.08h, ..., and 0.13h, respectively. The natural frequencies of the first five modes for the notched plate are calculated using ABAQUS. Also, the first five natural frequencies of the ideal SFSF plate are estimated by ABAQUS in which mesh 3 is used. These frequencies are listed in Table 4.4 for comparison.

In order to judge which notch is the best, the root of mean square(RMS) of the

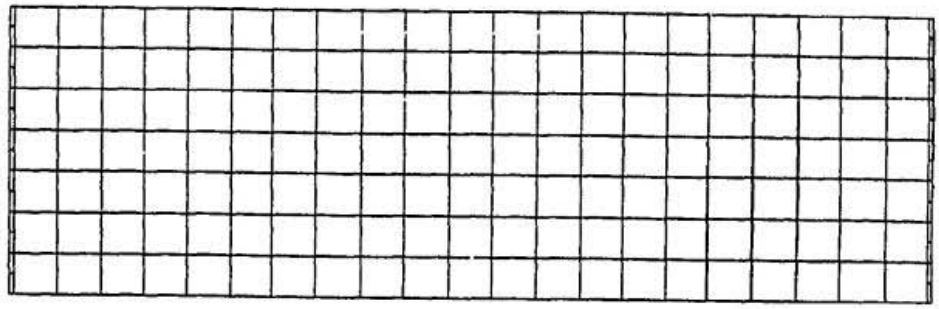

(a)

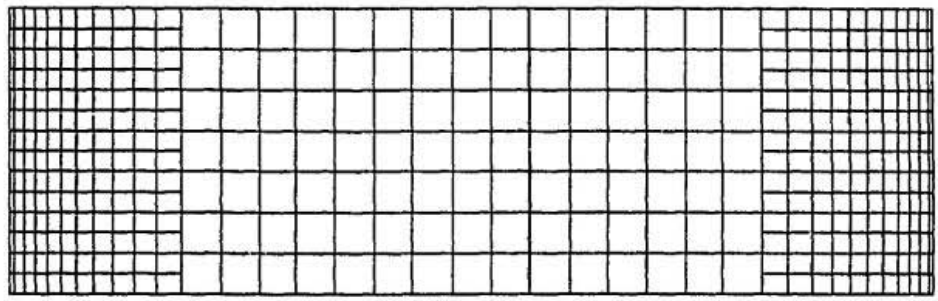

(b)

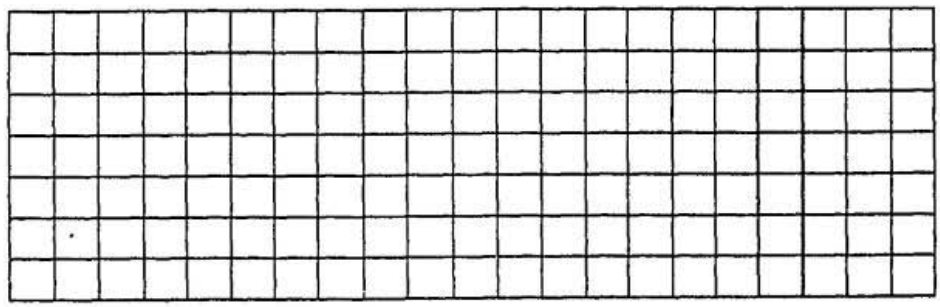

(c)

Figure 4.8: (a) Shell element mesh 1
(b) Shell element mesh 2
(c) Shell element mesh 3

Table 4.4: Natural frequencies(Hz) of the SFSF plate

Mode No.			1	2	3	4	5
Ideal SFSF			51.015	205.660	228.600	465.510	491.600
Simulated	†3mm	‡0.07	51.332	204.010	222.650	459.520	478.650
		0.08	51.741	204.570	223.700	460.630	480.920
		0.09	52.251	205.180	224.480	461.590	482.540
		0.10	52.871	205.880	225.090	462.520	483.810
		0.11	53.606	206.690	225.610	463.500	484.870
		0.12	54.460	207.630	226.110	464.570	485.820
		0.13	55.435	208.710	226.580	465.750	486.730
	4mm	0.07	50.932	202.600	218.670	455.150	469.840
		0.08	51.256	203.230	220.500	457.000	473.950
		0.09	51.652	203.820	221.780	458.350	476.760
		0.10	52.131	204.440	222.730	459.470	478.810
		0.11	52.700	205.110	223.490	460.490	480.400
		0.12	53.363	205.870	224.130	461.490	481.710
		0.13	54.124	206.720	224.690	462.540	482.840
SFSF	5mm	0.07	50.596	200.980	213.550	449.350	458.310
		0.08	50.877	201.810	216.520	452.470	465.080
		0.09	51.210	202.490	218.510	454.560	469.590
		0.10	51.606	203.120	219.950	456.110	472.780
		0.11	52.074	203.760	221.050	457.380	475.160
		0.12	52.619	204.430	221.930	458.500	477.030
		0.13	53.245	205.170	222.660	459.570	478.570

†notch width; ‡coefficient of the notch thickness.

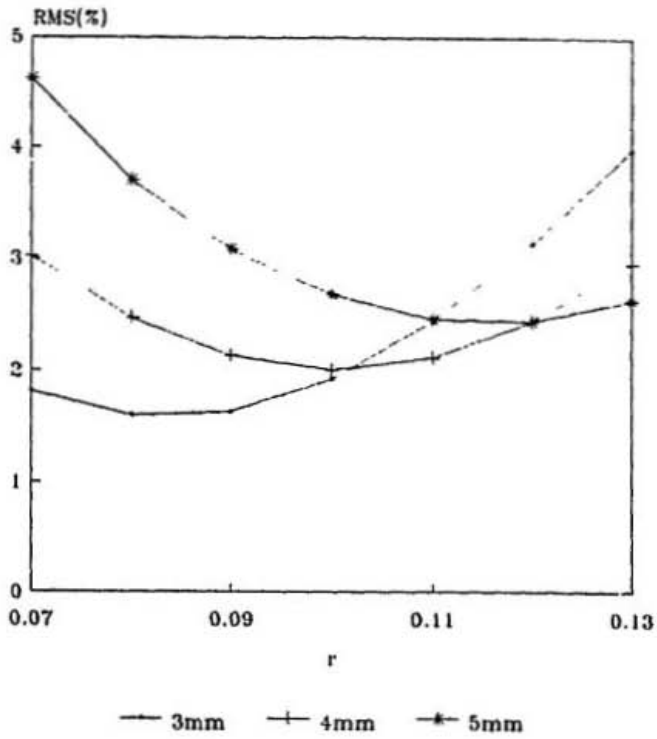

Figure 4.9: RMS versus notch dimensions

non-dimensionalized deviation(NDD) of each natural frequency for a simulated SFSF plate from the ideal one is estimated and shown in Figure 4.9, in which

$$NDD_i = \frac{f_i - f_i'}{f_i}$$

$$RMS = \sqrt{\frac{1}{5}\sum_{i=1}^{5} NDD_i^2}$$

where f_i and f_i' are the natural frequency of the i-th mode for an ideal SFSF plate and the simulated SFSF plate, respectively.

From Figure 4.9, it is found that, the minimum RMS 1.595% is obtained when the notch has a width of 3 mm and a depth of 0.7488 mm. However, considering the

notch strength, the handling convenience during the test, the difficulty in manufacturing and the sizes of the milling tools available, the notch is measured 3.2×0.936 mm. The natural frequencies of the first five modes for the notched plate are estimated in the same way, and the RMS is 1.885%.

Natural frequencies are one aspect of concern; another one is the concurrence in mode shapes between the ideal and simulated SFSF plates. Figures 4.10 and 4.11 show the mode shapes of the two plates. It is found that mode shapes of the first five mode for the two plates are in good agreement with each other. The consensus of natural frequencies and mode shapes indicates that the simulated SFSF plate is a good approach to the ideal SFSF plate.

4.4 General Procedures of Experiments

The experiment was performed firstly to the CFCF plate then the SFSF plate both in air and in water. For the experments in water, the depth of submersion above the plates h_1 varied from 0 to 327.5 mm in five steps while the water level below the plates remained 275 mm. The driving point was located at 327.50 mm from each end, 30 mm off center; the responses of the plates were collected only at acquisition points of the $\frac{3}{4}$ plate area because of the symmetry of the plates, as shown in Figure 4.12. The positions of these points were determined, based on the predicted dynamic behaviour of the plates in the first five modes, so that all of the modal responses could be obtained.

Each test was performed in two steps. Firstly, sinusoidal sweep excitation with normal frequency span 200Hz was done to roughly locate the resonant frequency for the first five modes. Secondly, sinusoidal sweep excitation with frequency span 50Hz

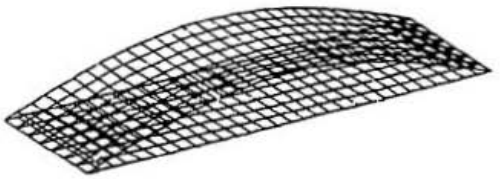

51.02Hz

205.60Hz

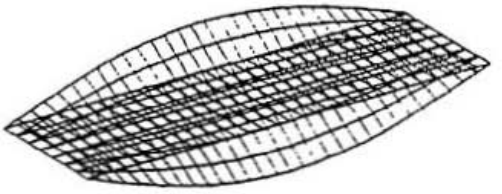

228.60Hz

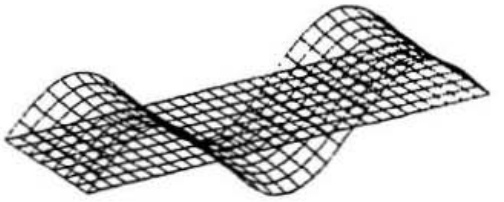

465.51Hz

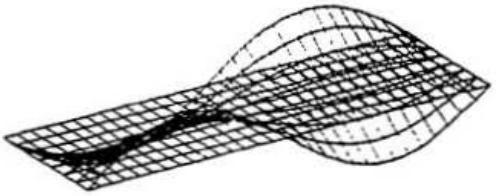

491.60Hz

Figure 4.10: Mode shapes of the ideal SFSF plate

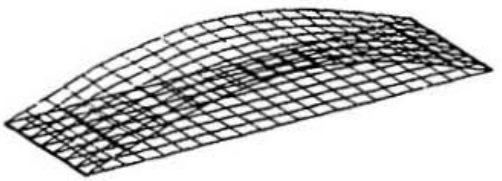

52.70Hz

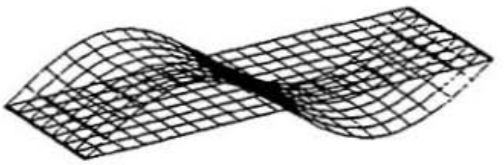

205.57Hz

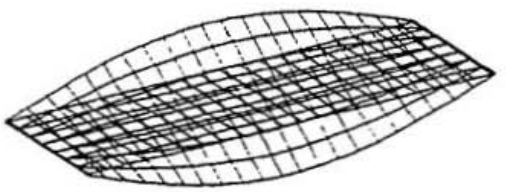

224.59Hz

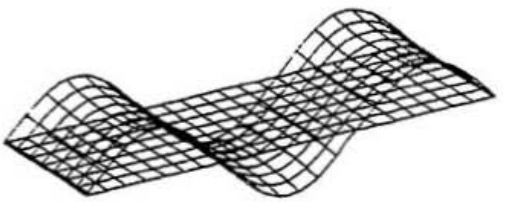

461.87Hz

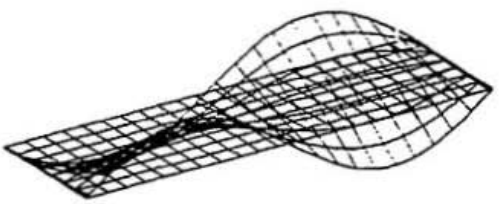

482.79Hz

Figure 4.11: Mode shapes of the simulated SFSF plate
– notch size: $3.2 \times 0.936mm$

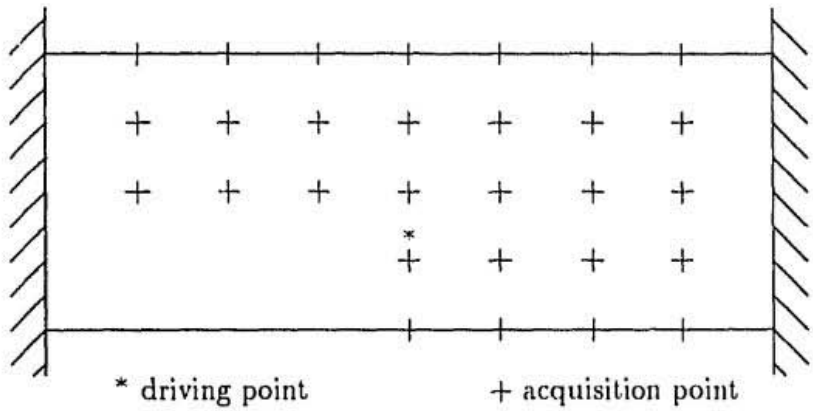

Figure 4.12: The distribution of the driving point and acquisition points

around each resonant frequency was performed to obtain frequency response functions so that modal parameters could be identified. In both sweep excitations, the average number was 20 and the sweep time was 1.8 seconds. The frequency response function at each acquisition point was obtained by the analyzer and stored in the PC computer.

4.5 Modal Parameter Estimation

By using STAR software package, modal parameters of CFCF and SFSF plates both in air and in water are identified from the measured data. It is noted that the mode shape values at the points where the response has not collected are estimated by using the responses of symmetrical and anti-symmetrical points. The natural frequencies and modal damping ratios are tabulated in Tables 4.5 and 4.6. Because the mode shapes of the plates in water have not shown discernible variations from those in air, only the modal shapes of the plates in water are displayed, as shown in Figures 4.13 and 4.14.

Table 4.5: Modal frequencies and modal damping ratios of the CFCF plate

Mode	*Number* / *Type*		1 1st †bd.	2 1st ‡ts.	3 2nd bd.	4 2nd ts.	5 3rd bd.
In Air		Freq.(Hz) Damp.(%)	100.348 0.1850	244.986 0.2617	279.089 0.1874	522.486 0.1694	536.104 0.1965
Partial Submersion		Freq.(Hz) Damp.(%)	69.505 0.553	203.310 0.3185	205.382 0.5886	435.175 0.2267	405.725 0.5474
Full Submersion	*0.1	Freq.(Hz) Damp.(%)	59.828 0.6258	180.961 0.3356	174.240 0.6970	388.723 0.3303	353.397 0.5614
	0.2	Freq.(Hz) Damp.(%)	58.155 0.7106	179.574 0.3462	172.700 0.6983	385.894 0.3668	346.815 0.5741
	0.3	Freq.(Hz) Damp.(%)	57.837 0.742	179.218 0.3605	169.501 0.7055	385.874 0.3870	345.300 0.5897
	0.4	Freq.(Hz) Damp.(%)	57.510 0.765	179.158 0.3622	167.250 0.70.73	385.845 0.4339	345.233 0.5947
	0.5	Freq.(Hz) Damp.(%)	57.444 0.7812	179.152 0.3664	167.010 0.7079	385.739 0.4531	344.999 0.5977

†bd.–bending mode; ‡ts.– torsional mode; *$\frac{h_1}{a}$.

Table 4.6: Modal frequencies and modal damping ratios of the SFSF plate

Mode	*Number* / *Type*		1 1st †bd.	2 2nd bd.	3 1st ‡ts.	4 3rd bd.	5 2nd ts.
In Air		Freq.(Hz) Damp.(%)	50.871 0.1947	198.500 0.2115	211.448 0.2598	442.750 0.2501	455.832 0.2295
Partial Submersion		Freq.(Hz) Damp.(%)	34.520 0.5191	145.468 0.8338	176.400 0.3165	334.636 0.5489	380.993 0.3043
Full Submersion	*0.1	Freq.(Hz) Damp.(%)	30.100 0.5448	125.500 0.8867	155.873 0.3225	288.125 0.0.5930	338.638 0.3365
	0.2	Freq.(Hz) Damp.(%)	29.294 0.5739	121.250 0.9146	154.670 0.3365	283.125 0.6207	335.367 0.3744
	0.3	Freq.(Hz) Damp.(%)	28.910 0.5891	119.250 0.9526	154.569 0.3428	282.410 0.6434	334.667 0.4424
	0.4	Freq.(Hz) Damp.(%)	28.800 0.6062	117.250 0.9562	154.500 0.3494	281.870 0.6855	335.320 0.4433
	0.5	Freq.(Hz) Damp.(%)	28.723 0.6126	117.125 0.9754	154.510 0.3572	281.795 0.7080	335.040 0.4453

†bd.–bending mode; ‡ts.– torsional mode; *$\frac{h_1}{a}$.

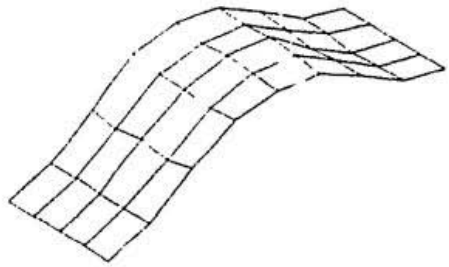

57.444Hz

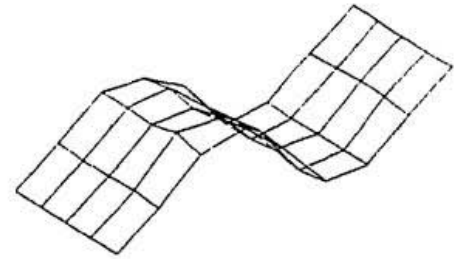

167.01Hz

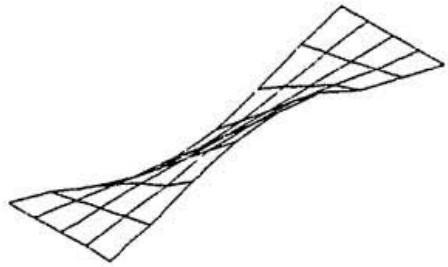

179.152Hz

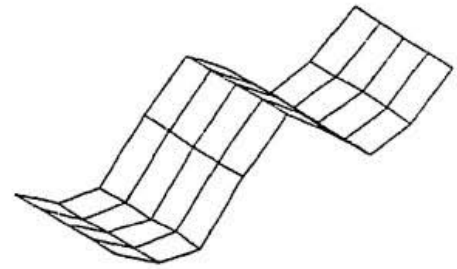

344.999Hz

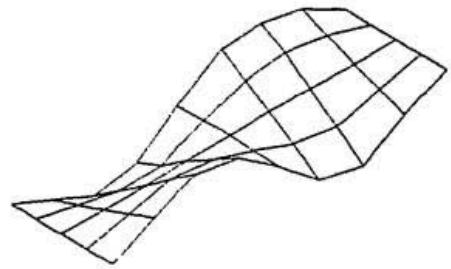

385.739Hz

Figure 4.13: Mode shapes of the CFCF plate in water

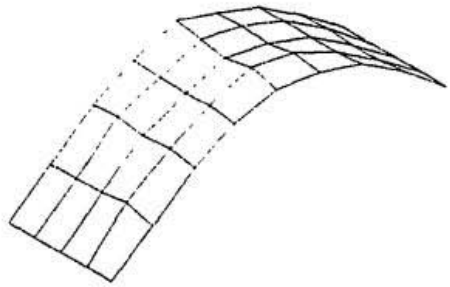

28.723Hz

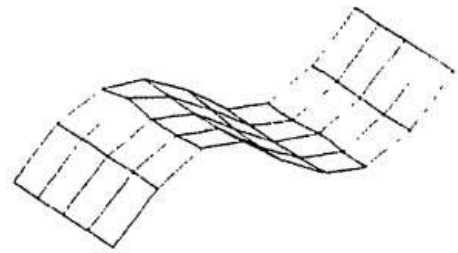

117.125Hz

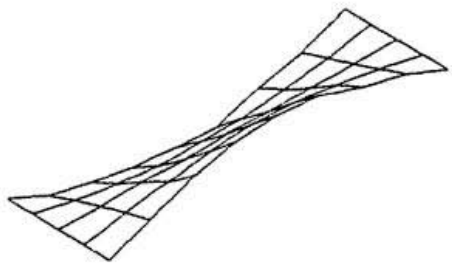

154.510Hz

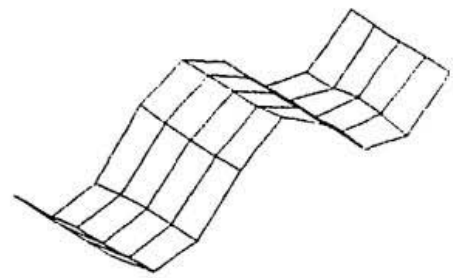

281.795Hz

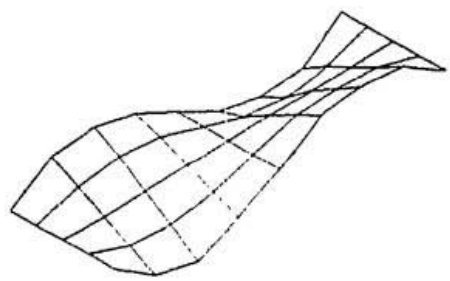

335.040Hz

Figure 4.14: Mode shapes of the SFSF plate in water

Table 4.7: Natural frequencies(Hz) of the CFCF plate in air

Mode	*ABAQUS*	*Experiment*	*Deviation(%)*
1	117.99	100.348	14.952
2	269.52	244.986	9.103
3	324.66	279.089	14.037
4	576.77	522.486	9.412
5	636.68	536.104	15.797

4.6 Discussion

4.6.1 Experiments in Air

The natural frequencies of the first five modes for the CFCF and SFSF plates obtained using the finite element software ABAQUS are given in Tables 4.7 and 4.8. Experimental values are also given in the same tables. It is found, for the CFCF plate, that the maximum deviation of 15.797% is present while less than 6% deviation exists in the SFSF plate.

The relatively good agreement between the experiment and the FEM obtained for the SFSF plate affirms that the notched plate with clamped ends is a good approach to the SFSF plate.

The discrepancy in the estimation of the frequency between the two methods may be explained by the following two aspects. On one hand, any decrease in the actual support rigidity from the infinite value assumed in the finite element method or slippage at the fixed ends will lead to a decrease in natural frequencies. The effect of support strains or slippage in fixed supports is similar to that of increasing the

Table 4.8: Natural frequencies(Hz) of the SFSF plate in air

	Ideal SFSF	*Simulated SFSF*		
Mode	*ABAQUS*	*ABAQUS*	*Experiment*	*Deviation(%)*
1	51.02	52.70	50.871	3.463
2	205.60	205.57	198.500	3.439
3	228.60	224.59	211.448	5.852
4	465.51	461.87	442.750	4.140
5	491.60	482.79	455.832	5.584

length, by an amount ranging from close to zero to a maximum of about one half the plate thickness for one fixed end[Donnell, 1976]. This effect is more critical for the CFCF plate than for the SFSF plate, because the notches greatly decrease the rigidity demand for the fixed ends.

On the other hand, the experimental values are generally lower than that obtained by the FEM as a result of the finite density of the air and the fact that the frequencies from the finite element method are upper bounds, since the stiffness of the plate was overestimated by use of the finite element method. Also, it should be pointed out that the range of 0.30mm deviation exists in the plate thickness so that the assumptions of uniform plates in the finite element method is deviated.

4.6.2 Experiments in Water

It is observed that due to the presence of the fluid, natural frequencies of vibrating plates decrease and modal damping ratios increase. However, mode shapes have not shown discernible change, and node lines remain in their original position. The following comments may explain the reasons. In the experiments, the plates are

placed symmetrically in the tank both in the x and y directions. The water effect on the plates can be modeled as the added mass and the increase in damping ratios while the stiffness remains the same as that in air. However, the increase in the density and damping ratios does not change symmetry of the system. Because of the system symmetry, both the chordwise node lines and the spanwise node lines will remain in their original positions.

Natural Frequencies

Table 4.9 shows the percentage change in the natural frequencies when the plates are submerged in water. Where the values are calculated by

$$\frac{f_{fluid} - f_{air}}{f_{air}} \times 100\%$$

The results in Table 4.9 show that the depth of submergence has approximately the same effect irrespective of the type of boundary conditions. To illustrate this, let us consider the first bending mode. Once the plates come in contact with water, one sees a decrease in the first natural frequency of about 30%. As the depth increases, the rate of decrease in the natural frequency diminishes until a certain depth is reached beyond which the natural frequency does not change. One also notices that the change in the natural frequency is slightly greater in the case of the SFSF plate than in the case of the CFCF plate.

More interesting characteristics will be found if the non-dimensionalized value, added mass factor(AMF), is used to measure the frequency change due to the fluid effect. According to the discussion in Chapter 3, the AMF can be determined from natural frequencies of tested plates in air and in fluid. The increase in the added mass

Table 4.9: Percentage decrease in natural frequencies of plates in water

Mode type			1st †bd.	2nd bd.	3rd bd.	1st ‡ts.	2nd ts.
CFCF	*Partial Submersion*		30.736	26.410	24.320	17.012	16.711
	Full Submersion	*0.1	40.379	37.568	34.081	26.134	25.601
		0.2	42.047	38.120	35.308	26.700	26.143
		0.3	42.364	39.266	35.591	26.846	26.147
		0.4	42.689	40.073	35.603	26.870	26.152
		0.5	42.755	40.159	35.647	26.873	26.172
SFSF	*Partial Submersion*		32.142	26.717	24.419	16.575	16.418
	Full Submersion	0.1	40.831	36.776	34.924	26.283	25.710
		0.2	42.415	38.917	36.053	26.852	26.427
		0.3	43.170	39.924	36.215	26.900	26.581
		0.4	43.386	40.932	36.337	26.932	26.438
		0.5	43.538	40.995	36.353	26.928	26.499

†bd.–bending mode; ‡ts.– torsional mode; *$\frac{h_1}{a}$.

factors, which is equivalent to a decrease in the natural frequencies, is estimated using Equation.3.26. These data have been plotted in Figures 4.15 and 4.16, where the value coinciding to $\frac{h_1}{a} = 0$ corresponds to the case of partial submersion.

Figures 4.15 and 4.16 display the following features:

(i) Added mass factors increase with the increase of the depth of submergence for all modes; however, they approach to limiting values with the increase in the depth of submergencce. This indicates that the effect of the free fluid surface on the plates attenuates as the distance from the plates becomes large. Moreover, the limiting values of AMFs for the bending modes are generally approached at a deeper submergence than that for the torsional modes.

(ii) Added mass factors have strong dependence on the mode shape type. Bending modes have much higher AMFs than the torsional modes do. Let us take the added mass factors of the CFCF plate when it is fully and deeply submerged in water as the example. The limiting value is 2.052 for the first bending mode while the corresponding value for the first torsional mode is 0.870.

For torsional modes, the fluid dynamic pressure produces effect on the vibrating plate in the form of moment instead of force as in bending modes. Thus the arm of force is also a factor to govern the fluid effect in torsional modes. However, the aspect ratio(the ratio of width to length) of the plates is 0.308; so the small arm of force results in a small perturbation to the fluid field and added mass factors for the torsional modes.

(iii) For the same mode type, added mass factors have dependence on the mode order. The lower the mode order, the higher the added mass factor. The

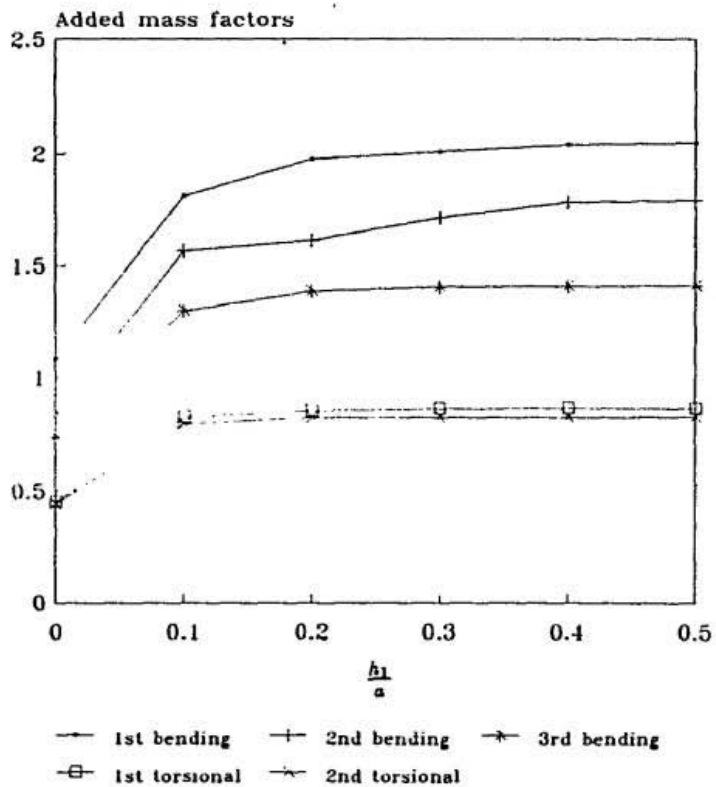

Figure 4.15: Added mass factors versus $\frac{h_1}{a}$ for the CFCF plate

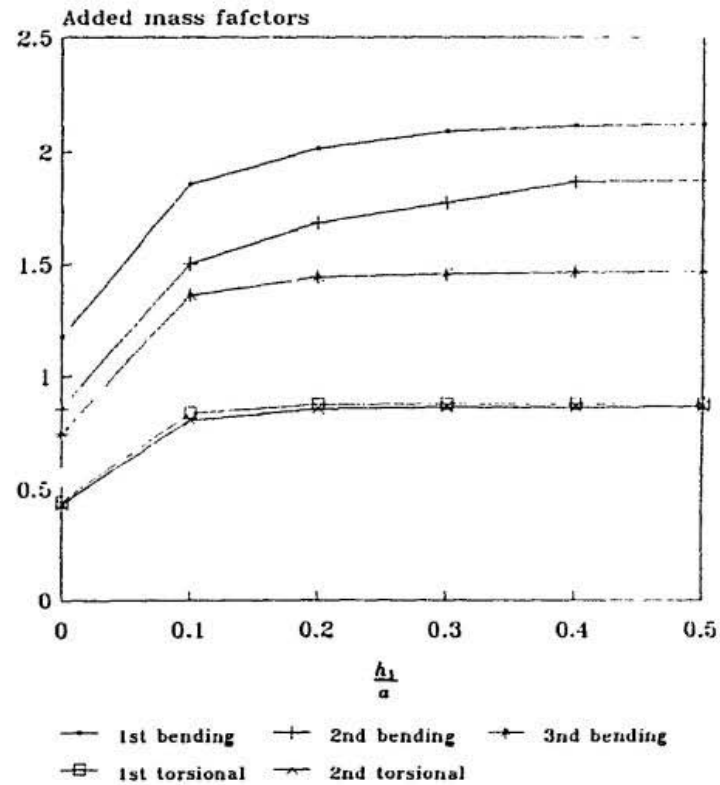

Figure 4.16: Added mass factors versus $\frac{h_1}{a}$ for the SFSF plate

higher the mode order, the lower the depth of submergence at which the AMF approaches its limiting value. This is in agreement with the results obtained by Fu and Price[1987].

Let us take the bending modes of the CFCF plate to illustrate. The limiting value of the AMF for the first mode is 1.144 times that of the second mode, and 1.450 times that of the third mode. Because of the higher inertia of the fluid, its response to high-frequency vibrations is less than its response to low-frequency vibrations. Thus this results in the surrounding layer of fluid, involved in motion by the vibrating plate, becomes thinner than that of the plate vibrating at a low-frequency.

The limiting values of the AMF for the first bending mode is obtained when $\frac{h_1}{a}$ reaches 0.5 or even higher, while the constants for the second and third bending modes are obtained when $\frac{h_1}{a}$ is about 0.4 and 0.3, respectively. As stated earlier, as the fluid layer involved in motion by the vibrating plate is determined by the vibrating frequency, further increase of submergence level does not bring more fluid into motion after the depth of submergence has approached to a certain value.

(iv) Added mass factors increase abruptly once the plates come in contact with water. Let us consider the bending modes of the CFCF plate. When the plate is partially submerged in water, the added mass factor is 1.084, 0.847, and 0.746 for the first, second and third bending modes, respectively. These values are almost equal to half of their limiting values. This phenomenon seems to show that both free fluid surface and the water tank bottom have approximately equal effects on the submerged vibrating plate when it is far from these boundaries.

Besides, it is also observed that the fluid effect alters the mode order and the extent of mode-coupling of the CFCF plate. This results from a unequal decrease of natural frequencies in bending modes and torsional modes due to the presence of water. When the plate is submerged in water, the third mode and fifth mode of the plate in air whose modal frequencies are 279.089Hz and 536.104Hz shift to the second and forth modes, respectively, as shown in Table 4.5. Also, when the plate is in air, the second and the third modes are uncoupled/lightly-coupled(peak difference is 34.103Hz). However, these two modes become heavily coupled(peak difference is 2.072Hz) when it is partially submerged in water.

Modal Damping Ratios

The increase in modal damping ratios due to fluid effect when the plates are submerged in water are estimated by

$$\frac{\xi_{fluid}}{\xi_{air}}$$

and plotted in Figures 4.17 and 4.18, where ξ_{air} and ξ_{fluid} are the modal damping ratios of the plates in air and in water; the value coinciding with $\frac{h_1}{a} = 0$ corresponds to the case of partial submergence. Several features are shown:

(i) The modal damping ratio increases due to the presence of the fluid, but approaches to a limiting value as the depth of submergence increases. When the plates are fully and deeply submerged in water($\frac{h_1}{a}$=0.5), the maximum increase of 3.61 times is observed, which occurs to the second bending mode of the SFSF plate.

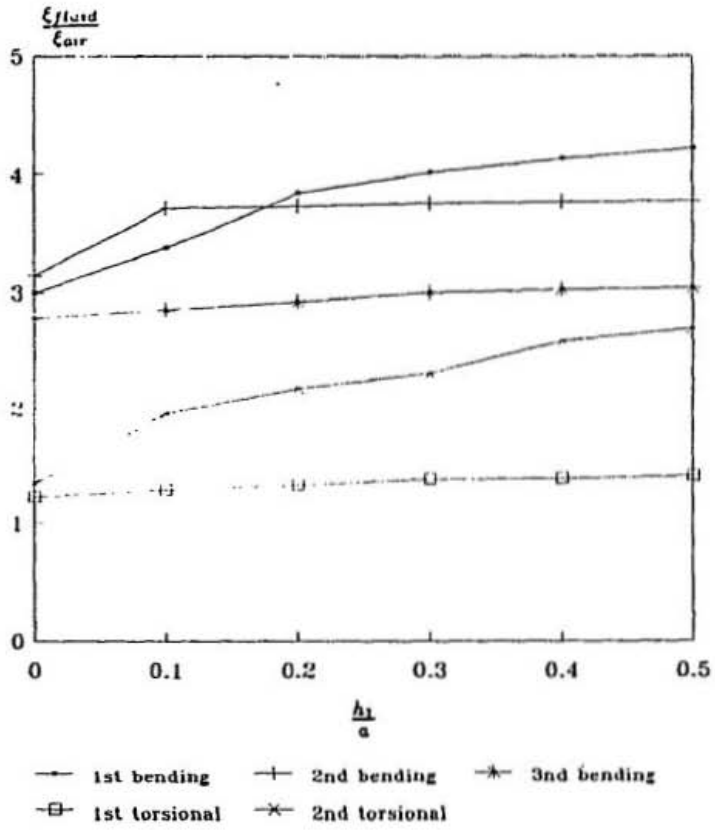

Figure 4.17: The increase in modal damping ratios for the CFCF plate

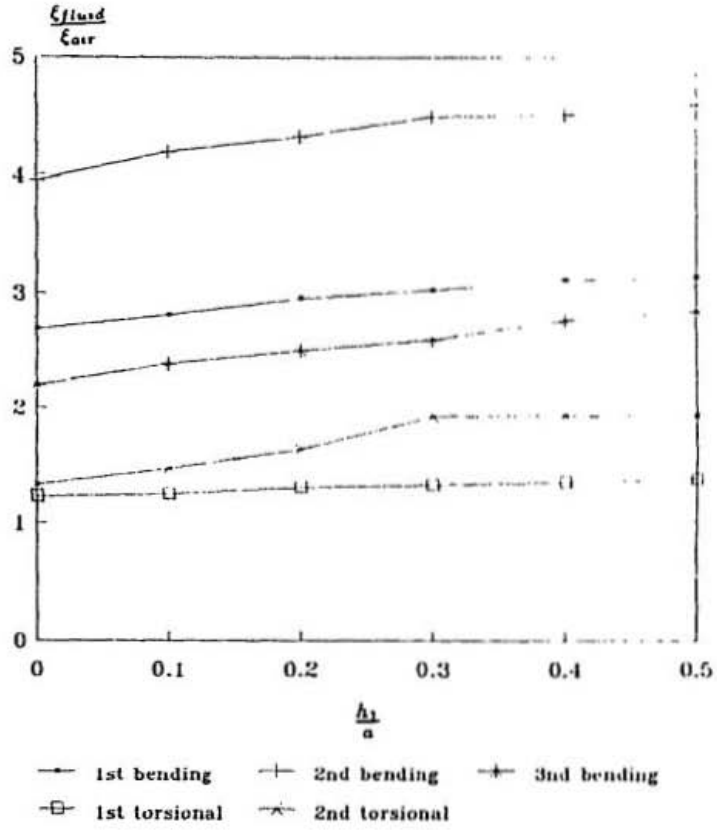

Figure 4.18: The increase in modal damping ratios for the SFSF plate

(ii) Similar to added mass factors, the modal damping ratios have strong dependence on the mode shape type. The modal damping ratio for the bending modes exhibit greater increases than that of torsional modes when the plates are submerged in water. When the SFSF plate is fully and deeply submerged in water($\frac{h_1}{a}$=0.5), the modal damping ratio for the first bending mode increases to 3.15 times while the damping ratio for the first torsional mode increases to 1.37 times.

4.6.3 Fluid Effect versus Plate Boundary Conditions

As stated earlier, the fluid effect on the vibrating plates causes the decrease in natural frequencies and the increase in modal damping ratios. However, this effect varies between the two plates because of the variation in their boundary conditions.

From Figures 4.15 and 4.16, it is observed that boundary conditions show little effect on added mass factors of torsional modes. For the CFCF plate, the limiting values of AMFs are 0.870 and 0.835 for the first and second torsional modes, respectively, which compares with the corresponding values of 0.883 and 0.870 for the SFSF plate.

However, the effect of boundary condition on added mass factors of bending modes is distinct. To illustrate this, let us see the first bending mode. The limiting value of the AMF for the SFSF plate is 2.127 while the corresponding value for the CFCF plate is 2.052.

This occurrence might be illustrated using the plate theory. It is boundary conditions that determine the frequency equation of the plate. Thus the boundary conditions govern fluid-loading effect through natural frequencies. From Tables 4.5

and 4.6, it is observed that SFSF plate has lower corresponding natural frequencies than the CFCF plate does. This makes the SFSF plate involve a thicker layer of fluid around it into motion. Thus a greater added mass factor results in.

On the other hand, the effect of boundary conditions on modal damping ratios is not as distinct as expected. It may be the complexity of the fluid motion that overwhelms this trend.

4.7 Summary

A notched plate with clamped ends is suggested to simulate the SFSF plate, and finite element software ABAQUS is used to optimize the dimensions of the notch. Experiments are carried out on the CFCF and SFSF plates both in air and in water at six different depths of submergence, respectively. Experimental study on the plates in air demonstrates that the tested plates are good models of the CFCF and SFSF plates. It is found, from the experimental study on the plates in water, that the fluid effect on the submerged vibrating plates has two aspects, the decrease in natural frequencies and the increase in modal damping ratios. Mode shapes have not shown discernible changes due to the presence of fluid.

The added mass, which is used to account for the fluid-loading effect, and the increase in modal damping ratios due to the presence of fluid have been evaluated for the first five modes of the two plates. Several important characteristics on the added mass and modal damping ratios have been clearly illustrated. The effect of the plate boundary conditions on the added mass factors and the increase in modal damping ratios of the plates is also

Chapter 5

Analytical Study

As stated earlier, analytical solutions to the fluid-plate interaction problems, in which the plate is in contact with fluid on one side, exist in the literature. However, the problem in which the plate is loaded by fluid on two sides has not been considered before. Also, no study of the effect of the depth of submergence above and below the plate on the response of the vibrating plate has been reported.

In this chapter, a plate loaded by fluid on two sides is considered. The analytical solution to the vibrating rectangular plate submerged in fluid is sought. The approach is applied to the CFCF and SFSF plates and assessed using results obtained by the experimental study of Chapter 4.

5.1 Formulation of the Problem

An uniform, flat, horizontally placed plate, submerged in a body of fluid is considered, as shown in Figure 5.1 The plate undergoes small-amplitude free bending vibration. The fluid motion due to the vibration of the plate produces dynamic pressures $p_U(x, y, t)$ and $p_L(x, y, t)$ on the upper and lower fluid-plate interfaces S_U and S_L, respectively.

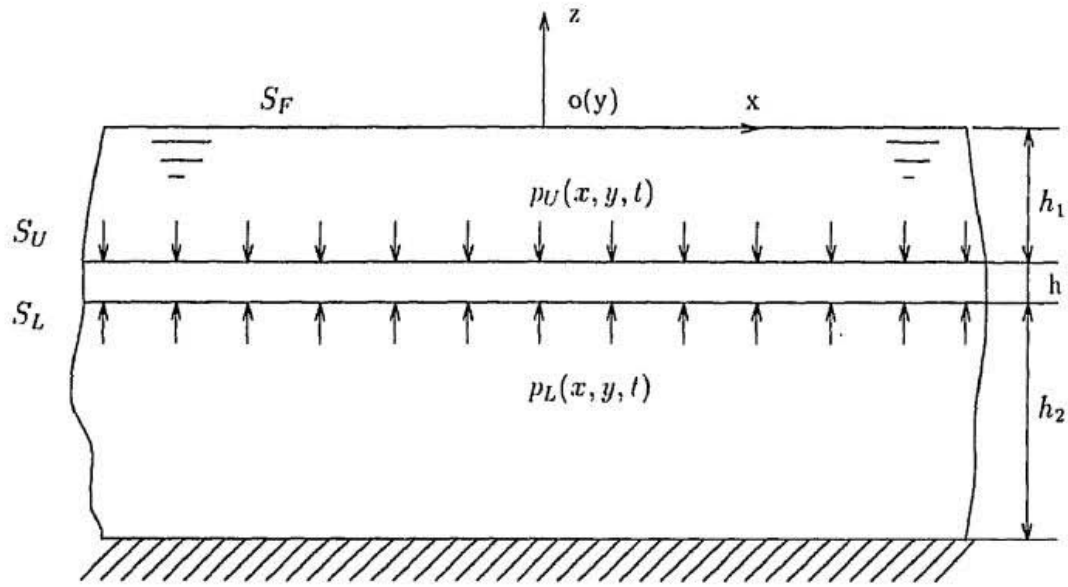

Figure 5.1: A rectangular plate submerged in a body of fluid

The plate of a length a, breadth b and thickness h has a constant mass per unit area m and flexural rigidity D, where $D = \frac{Eh^3}{12(1-\nu^2)}$, in which E is the Young's modulus of the plate material, ν is the Poisson ratio, and h is the thickness of the plate. For a small-amplitude bending vibration, where membrane stresses in the plate are negligible, the response of the plate is governed by, see Gorman [1982]

$$m\frac{\partial^2 W(x,y,t)}{\partial t^2} + D\nabla^4 W(x,y,t) = p_L(x,y,t) - p_U(x,y,t) \tag{5.1}$$

where W(x,y,t) is the upward displacement of the plate measured from its static equilibrium position.

The fluid, of density ρ_f, is assumed to be homogeneous, incompressible, inviscid and its motion irrotational. Thus, the velocity potential, $\phi(x,y,z,t)$ satisfies Laplace's equation, given by

$$\nabla^2 \phi(x,y,z,t) = 0 \tag{5.2}$$

Since the fluid motion is irrotational, the unsteady Bernoulli equation

$$\rho_f \frac{\partial \phi}{\partial t} + p + \frac{1}{2}\rho_f(\phi_x^2 + \phi_y^2 + \phi_z^2) + \rho_f g z = 0 \tag{5.3}$$

can be applied, where

$$\phi_x = \frac{\partial \phi}{\partial x}$$

$$\phi_y = \frac{\partial \phi}{\partial y}$$

$$\phi_z = \frac{\partial \phi}{\partial z}$$

Under the assumption that the plate undergoes a small-amplitude vibration, the resulting wave motion on the fluid surface is of small-amplitude also. Neglecting the nonlinear term $(\phi_x^2 + \phi_y^2 + \phi_z^2)$ for small-amplitude waves, Equation 5.3 can be replaced by its linearized form, i.e.,

$$\rho_f \frac{\partial \phi}{\partial t} + p + \rho_f g z = 0 \tag{5.4}$$

Since waves are assumed to be small, the linearized free surface boundary condition

$$\frac{\partial \phi}{\partial z} \mid_{z=0} - \frac{\omega^2}{g}\phi \mid_{z=0} = 0 \tag{5.5}$$

can be applied on S_F, where ω is the angular frequency of the wave motion caused by the vibration of the plate.

On the bottom of the tank, the normal component of velocity is zero, i.e.,

$$\frac{\partial \phi}{\partial z} \mid_{z=-(h_1+h+h_2)} = 0 \tag{5.6}$$

At the plate-fluid interfaces S_L and S_U, the kinematic boundary conditions are given by

$$\frac{\partial \phi}{\partial z} \mid_{z=-(h_1+h)} = \frac{\partial \phi}{\partial z} \mid_{z=-h_1} = \frac{\partial W}{\partial t} \tag{5.7}$$

Using Equation 5.4, we have

$$\rho_f \frac{\partial \phi}{\partial t} \mid_{z=-h_1} + p_U - \rho_f g h_1 = 0 \quad on \quad S_U \tag{5.8}$$

$$\rho_f \frac{\partial \phi}{\partial t} \mid_{z=-(h_1+h)} + p_L - \rho_f g (h_1 + h) = 0 \quad on \quad S_L \tag{5.9}$$

Substitution of Equations 5.8 and 5.9 into Equation 5.1 gives the following governing equation

$$m \frac{\partial^2 W}{\partial t^2} + \rho_f [\frac{\partial \phi}{\partial t} \mid_{z=-(h_1+h)} - \frac{\partial \phi}{\partial t} \mid_{z=-h_1}] + D \nabla^4 W - \rho_f g h = 0 \tag{5.10}$$

5.2 Solution of the Problem

Consider now the response of the fluid and the plate in any one combined mode. The displacement of the small-amplitude bending vibration of the plate can be assumed as

$$W(x, y, t) = \overline{W}(x, y) T(t) \tag{5.11}$$

We will also assume the velocity potential $\phi(x, y, z, t)$ in the form of

$$\phi(x, y, z, t) = G(x, y) F(z) S(t) \tag{5.12}$$

Substituting Equation 5.12 into Equation 5.2 gives

$$F(z) \nabla^2 G(x, y) + G(x, y) \frac{d^2 F(z)}{dz^2} = 0 \tag{5.13}$$

$G(x,y)$ is a function of x and y, and $F(z)$ is a function of z, so the following equation holds, viz.,

$$\frac{\nabla^2 G}{G} = -\frac{\frac{d^2F}{dz^2}}{F} = -\mu^2 \tag{5.14}$$

which can be written as

$$\nabla^2 G + \mu^2 G = 0 \tag{5.15}$$

$$\frac{d^2F}{dz^2} - \mu^2 F = 0 \tag{5.16}$$

where μ^2 is a real constant, and μ is the plane wave number, which is determined by the vibrating frequency of the submerged plate and fluid boundary conditions in the x-y plane.

Substituting Equations 5.11 and 5.12 into Equation 5.7 gives

$$G(x,y)S(t) = \overline{W}(x,y)\frac{\dot{T}}{F'|_{z=-(h_1+h)}} \tag{5.17}$$

where

$$\dot{T} = \frac{dT}{dt}$$

$$F'(z) = \frac{dF}{dz}$$

Applying Equation 5.17 to Equation 5.12 gives

$$\phi(x,y,z,t) = F(z)\overline{W}(x,y)\frac{\dot{T}(t)}{F'|_{z=-(h_1+h)}} \tag{5.18}$$

We also have

$$\phi(x,y,z,t) = F(z)\overline{W}(x,y)\frac{\dot{T}(t)}{F'|_{z=-h_1}} \tag{5.19}$$

The combination of Equations 5.11, 5.18, 5.19 and Equation 5.10 gives

$$\ddot{T} + \omega_{fluid}^2 T = 0 \tag{5.20}$$

and

$$\nabla^4 \overline{W} - \beta^4 \overline{W} = 0 \tag{5.21}$$

Details of the derivations of Equations 5.20 and 5.21 are given in Appendix A, where ω_{fluid} is the natural frequency of the plate submerged in fluid; β is a constant determined by the plate boundary conditions. ω_{fluid} can be expressed as

$$\omega_{fluid}^2 = \frac{D\beta^4}{m + m^*} \tag{5.22}$$

where

$$m^* = \rho_f [\frac{F}{F'} \mid_{z=-(h_1+h)} - \frac{F}{F'} \mid_{z=-h_1}] \tag{5.23}$$

m^* is called the added mass due to the fluid-loading effect.

Solving Equation 5.21 subject to the boundary conditions of the plate yields the values of β and ω_{fluid} as well as the mode shapes. However, the previous experimental work done in the field of fluid-structure interaction has confirmed that the dynamic loading of the fluid has an insignificant effect on mode shapes of submerged plates, see Espinosa[1984] and Barone and Gallego-Juarez[1972]. The experimental study involved in this work also demonstrates this point. Thus, it is reasonable to apply this assumption in the analysis hereafter. Under this assumption, the dynamic analysis of a plate submerged in fluid is reduced simply to the determination of the added mass and changes in natural frequencies and damping ratios due to fluid effect. However, the change in damping ratios is not considered in the analytical study because of the assumption for the fluid. Thus the change in the natural frequencies of the plate can be subsequently estimated once the added mass has been evaluated.

If the plate vibrates in air, the response equations corresponding to Equations

5.20 and 5.21 can be obtained by assuming $m^* = 0$. i.e.,

$$\ddot{T} + \omega_{air}^2 T = 0 \tag{5.24}$$

$$\nabla^4 \overline{W} - \beta'^4 \overline{W} = 0 \tag{5.25}$$

where

$$\beta'^4 = \frac{\omega_{air}^2 m}{D} \tag{5.26}$$

and ω_{air} is the natural frequency of the plate in air.

The constant β' is determined by plate boundary conditions, which are the same whenever the plate is submerged in fluid or in air. Thus one has

$$\beta = \beta'$$

so

$$\omega_{fluid} = \omega_{air} \frac{1}{\sqrt[2]{1 + \frac{m^*}{m}}} \tag{5.27}$$

Equation 5.27 displays the relationship between natural frequencies of the plate in fluid and that in air. Obviously, the added mass m^* due to fluid-loading effect is the only element to be estimated. The non-dimensional quantity, $\frac{m^*}{m}$ in Equation 5.27 is defined as the added mass factor(AMF), which is also used to account for the effect of the surrounding fluid on the vibrating plate.

5.3 The Added Mass of a Plate Submerged in Fluid

Equation 5.23 shows that the value of the added mass can be obtained once the function F(z) has been solved using Equation 5.16. $\phi(x, y, z, t)$, and consequently F(z),

are not continuous at the fluid-plate interfaces due to the presence of the vibrating plate. So it is appropriate to evaluate F(z) by considering the two bodies of fluid individually, the fluid fields above and below the plate. The functions corresponding to these two bodies of fluid are designated as $F_1(z)$ and $F_2(z)$, respectively.

5.3.1 The Fluid Field above the Plate (F_1)

Consider the equation corresponding to Equation 5.16

$$\frac{d^2F_1}{dz^2} - \mu^2 F_1 = 0 \tag{5.28}$$

subject to the following boundary conditions:

(i) On the free fluid surface S_F where z=0, the linearized free surface boundary condition Equation 5.5 combined with Equation 5.12 gives

$$\frac{dF_1}{dz} \mid_{z=0} - \frac{\omega^2}{g} F_1 \mid_{z=0} = 0 \tag{5.29}$$

(ii) On the fluid-plate upper interface S_U where $z = -h_1$, the kinematic boundary condition Equation 5.7 combined with Equations 5.11 and 5.12 yields

$$F_1' \mid_{z=-h_1} = \frac{\overline{W}(x,y)\dot{T}}{G(x,y)S(t)} \tag{5.30}$$

Previous studies in the literature considered two extreme cases for the free surface boundary condition:

(i) The zero-frequency condition, $\omega = 0$, which yields

$$\frac{\partial \phi}{\partial z} \mid_{z=0} = 0$$

that is,

$$\frac{dF_1}{dz} |_{z=0} = 0$$

means that the vibrating plate is deeply submerged in fluid and the free fluid surface is static. This condition was applied by Lamb[1921] and McLachlan[1932] to a circular plate and corresponds to the infinite rigid wall condition.

(ii) Infinite frequency condition, $\omega \rightarrow \infty$, which yields

$$\phi |_{z=0} = 0$$

that is,

$$F_1 |_{z=0} = 0$$

This condition was applied by Kwak and Kim[1991] in solving a circular plate problem. The practical condition of ω is between these two extremes.

When the higher frequency limit is assumed, the previous equation reduces to $\phi = 0$ at the free surface, on which the pressure fluctuations due to the vibrating structure may be neglected[Hylarides and Vorus, 1982]. The imposition of this simplified condition immediately discards flexible structures with low natural frequencies, since in these cases the natural frequencies of the structure are most likely low. In this study, Equation 5.29 will be considered as the boundary condition to be satisfied on the free surface.

The general solution to Equation 5.28 is given by

$$F_1(z) = A_1 e^{\mu z} + A_2 e^{-\mu z} \tag{5.31}$$

where A_1 and A_2 are constants. A negative real constant, $-\mu^2$, is assumed on the right-hand side of Equation 5.14, so $F_1(z)$ cannot be represented as a trigonometric form, since the fluid disturbance should die out as we move away from the plate. Applying Equations 5.29 and 5.30 to Equation 5.31 gives

$$A_1 = \frac{g\mu + \omega^2}{\mu[(g\mu + \omega^2)e^{-\mu h_1} - (g\mu - \omega^2)e^{\mu h_1}]} \frac{\overline{W}(x,y)\dot{T}}{G(x,y)S(t)}$$

$$A_2 = \frac{g\mu - \omega^2}{\mu[(g\mu + \omega^2)e^{-\mu h_1} - (g\mu - \omega^2)e^{\mu h_1}]} \frac{\overline{W}(x,y)\dot{T}}{G(x,y)S(t)}$$

Thus a unique solution can be written as

$$F_1(z) = \frac{(C_1 e^{\mu z} + e^{-\mu z})(g\mu - \omega^2)}{\mu[(g\mu + \omega^2)e^{-\mu h_1} - (g\mu - \omega^2)e^{\mu h_1}]} \frac{\overline{W}(x,y)\dot{T}}{G(x,y)S(t)} \tag{5.32}$$

where

$$C_1 = \frac{g\mu + \omega^2}{g\mu - \omega^2} \tag{5.33}$$

5.3.2 The Fluid Field below the Plate (F_2)

Consider the equation corresponding to Equation 5.16

$$\frac{d^2F_2}{dz^2} - \mu^2 F_2 = 0 \tag{5.34}$$

subject to the boundary conditions:

(i) The boundary condition on the bottom of the tank, Equation 5.6 combined with Equation 5.12 becomes

$$\frac{dF_2}{dz}\Big|_{z=-(h_1+h+h_2)} = 0 \tag{5.35}$$

(ii) On the fluid-plate lower interface S_l where $z = -(h_1+h)$, the kinematic boundary condition, Equation 5.7 combined with Equations 5.11 and 5.12 yields

$$F_2' \mid_{z=-(h_1+h)} = \frac{\overline{W}(x,y)\dot{T}}{G(x,y)S(t)} \tag{5.36}$$

Similarly, a unique solution can be obtained as

$$F_2(z) = (C_2 e^{\mu z} + e^{-\mu z}) \frac{e^{-\mu(h_1+h+h_2)}}{\mu(e^{\mu h_2} - e^{-\mu h_2})} \frac{\overline{W}(x,y)\dot{T}}{G(x,y)S(t)} \tag{5.37}$$

where

$$C_2 = e^{2\mu(h_1+h_2+h)} \tag{5.38}$$

5.3.3 Added Mass Calculations

The added mass expressed by Equation 5.23 is comprised of two components, and each one of them is related to the fluid-loading effects from one body of fluid. Thus, the added mass m^* can be rewritten as

$$m^* = m_1^* + m_2^*$$

where

$$m_1^* = -\rho_f \frac{F_1}{F_1'} \mid_{z=-h_1} \tag{5.39}$$

$$m_2^* = \rho_f \frac{F_2}{F_2'} \mid_{z=-(h_1+h)} \tag{5.40}$$

Using Equations 5.32 and 5.39 yields the component m_1^* of the added mass

$$m_1^* = -\frac{\rho_f}{\mu} \frac{C_1 + e^{2\mu h_1}}{C_1 - e^{2\mu h_1}} \tag{5.41}$$

The added mass component m_2^* is obtained using Equations 5.37 and 5.40

$$m_2^* = \frac{\rho_f}{\mu} \frac{1 + e^{-2\mu h_2}}{1 - e^{-2\mu h_2}} \tag{5.42}$$

To use Equations 5.41 and 5.42 for the calculation of the added mass per unit area of the plate, m^*, one needs to determine the values of μ and C_1. This is discussed in the following sections.

Estimation of the Plane Wave Number μ

The experiments discribed in Chapter 4 are obtained using a finite rectangular plate submerged in a body of water contained in a finite tank. If we were to solve the potential flow problem, the following boundary conditions on the sides of the tanks would have to be satiisfied. These are

$$\frac{\partial \phi}{\partial x} |_{x=\pm \frac{L_1}{2}} = 0 \tag{5.43}$$

$$\frac{\partial \phi}{\partial y} |_{y=\pm \frac{L_2}{2}} = 0 \tag{5.44}$$

where L_1 and L_2 are the length and width of the tank, respectively. However, we will avoid solving the potential problem. Instead, we will find a value for μ based on a heuristic approach.

In the experiments described in Chapter 4, the natural frequencies of the plates were obtained from modal analysis of the plate response to an external excitation. This excitation produced plate vibrations in both bending and torsional modes. Let us see what happens when a torsional mode is excited in addition to the bending mode. It is reasonable to expect that the fluid motion in the x direction to be determined by the bending vibration of the plate. Thus, the value of μ_x is expected to equal to the modal wave number of the plate in the x direction, k_x. Also, because the CFCF and SFSF plates are freely supported in the spanwise edges, the modal wave number in the y direction, k_y corresponding to either one of the first three bending modes, is

equal to zero, thus one has

$$\mu_x = \beta$$

Since

$$\beta = \beta'$$

one has

$$\mu_x = \sqrt[4]{\frac{(2\pi f_{air})^2 m}{D}} \tag{5.45}$$

The torsional mode, on the other hand, will excite fluid motion in the y direction. The net result will be that the bending modes are coupled by torsional modes due to the fluid motion in the y direction.

The torsional vibration of the plate will produce two waves travelling in opposite directions. These waves will soon be reflected on the tank walls and will form a basic mode wave motion, which is a standing wave whose wave number μ_y depends only on the tank width. Thus,

$$\mu_y = \frac{2\pi}{L_2}$$

The net wave motion will be the sum of the wave motions in the x and y directions, with a plane wave number μ given by[Kundu, 1990]

$$\mu = \sqrt[2]{\mu_x^2 + \mu_y^2} \tag{5.46}$$

This value of μ can then be used in Equations 5.41 and 5.42.

This rationale is used to calculate the wave number for the different bending modes as shown in Table 5.1. In these calculations, the value of μ_y is kept constant

Table 5.1: Wave number of the CFCF and SFSF plates

	$^{\dagger}\mu_x$			μ		
Mode	1st ‡bd.	2nd bd.	3rd bd.	1st bd.	2nd bd.	3rd bd.
CFCF plate	6.5838	10.9798	15.2176	13.1853	15.8450	19.0285
SFSF plate	4.7051	9.2598	13.8294	12.3550	14.7055	17.9377

†The following values are used in the calculation:
(i) steel properties: $\rho = 7850kg/m^2$, E=$2.07 \times 10^{11} N/m^2$, $\nu = 0.3$;
(ii) the natural frequency of the plates in air f_{air} takes the values obtained by experimental method.

‡bd.-bending mode.

at

$$\mu_y = \frac{2\pi}{L_2}$$

where $L_2 = 0.55$ since the same transverse wave exists for the three bending modes.

Coefficient C_1

Consider the coefficient C_1 expressed by Equation 5.33

$$C_1 = \frac{g\mu + \omega^2}{g\mu - \omega^2} \tag{5.47}$$

which relates to the gravity acceleration g, angular frequency of the wave motion in fluid ω, and the wave number μ.

Obviously, the frequency of wave motion at the free fluid surface equals to the frequency at which a plate submerged in fluid vibrates. Thus when a plate vibrates at its natural frequency of one bending mode, one has

$$\omega = \omega_{fluid} = 2\pi f_{air}(1 + AMF)^{-\frac{1}{2}} \tag{5.48}$$

Wave number μ is determined using Equation 5.46 in which

$$\mu_y = \frac{2\pi}{L_2}$$

$$\mu_x = \sqrt{\frac{(2\pi f_{air})^2 m}{D}}$$

where

$$m = 7850 \times 9.36 \times 10^{-3} = 73.476 \quad kg/m^2$$

$$D = \frac{Eh^3}{12(1-\nu^2)} = \frac{2.07 \times 10^{11} \times (9.36 \times 10^{-3})^3}{12(1-0.3^2)} = 1554.45 \quad N/m$$

Substitution of μ and ω into Equation 5.47 gives $C_1 = f(AMF, f_{air})$. When AMF is equal to 0.5, 1.5, 2.5 and 3.5, respectively, the graph of C_1 versus f_{air} is plotted in Figure 5.2. It is observed that

$$C_1 \approx -1 \qquad when \quad f_{air} \geq 40Hz$$

The lowest natural frequency of the CFCF and SFSF plates in air is 50.871Hz, thus Equation 5.41 can be simplified to

$$m_1^* = \frac{\rho_f}{\mu} \frac{-1 + e^{2h_1\mu}}{1 + e^{2h_1\mu}} \tag{5.49}$$

5.4 Discussion of the Results

5.4.1 The Added Mass from the Fluid Field above the Submerged Plate

Substituting the values of μ given in Table 5.1 into Equation 5.49 gives the values of m_1^*. The non-dimensional added mass coefficient AMF_1 can then be plotted as

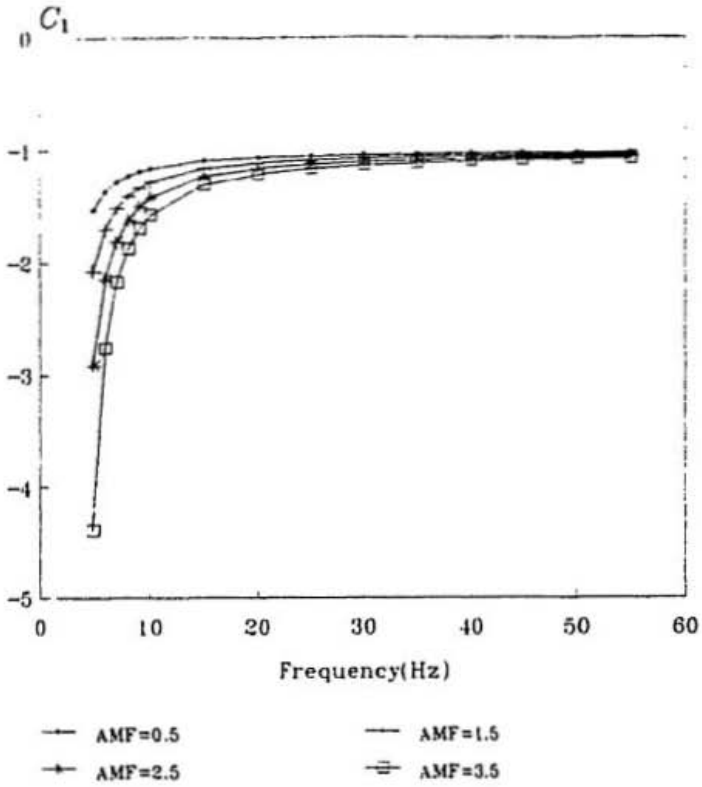

Figure 5.2: C_1 versus the natural frequency f_{air}

a function of the depth of submersion h_1. The relationship is shown in Figures 5.3 and 5.4 for the two plates CFCF and SFSF, respectively. The two curves portray the same general characteristics. For $\frac{h_1}{a}$ less than about 0.06, the non-dimensional added mass coefficient, AMF_1 increases linearly as the depth of submergence. The relationship then becomes nonlinear and the values of the AMF_1 for different modes taper off to constant values independent of the depth of submergence. The limiting value for the AMF_1 is higher for the lower bending vibration modes.

For the CFCF plate, the limiting values of AMF_1 are 1.03219, 0.85893 and 0.71523 for the first, second and third bending modes, respectively. The corresponding values for the SFSF plate are 1.10157, 0.92549 and 0.75872. However, for both plates,

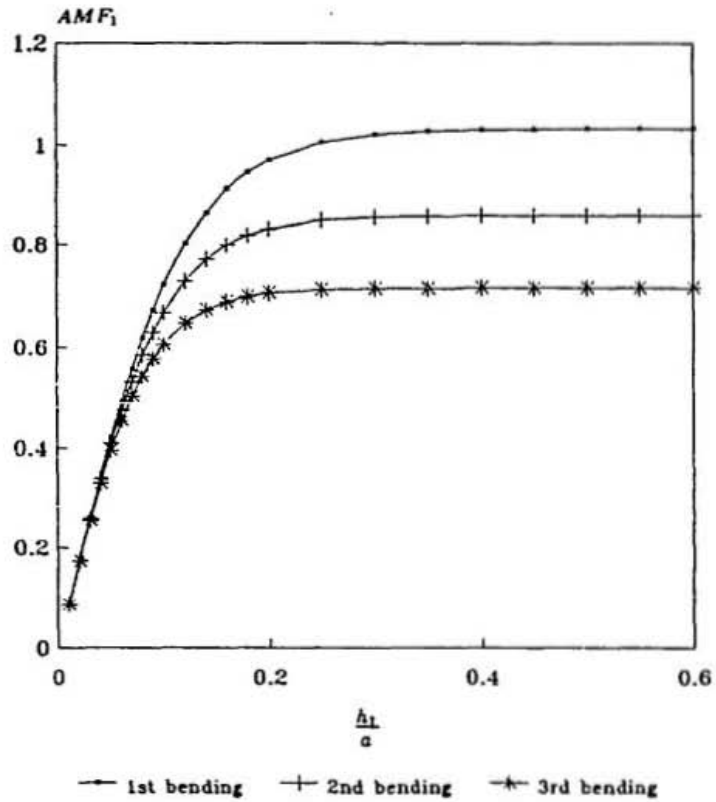

Figure 5.3: AMF_1 versus $\frac{h_1}{a}$ for the CFCF plate

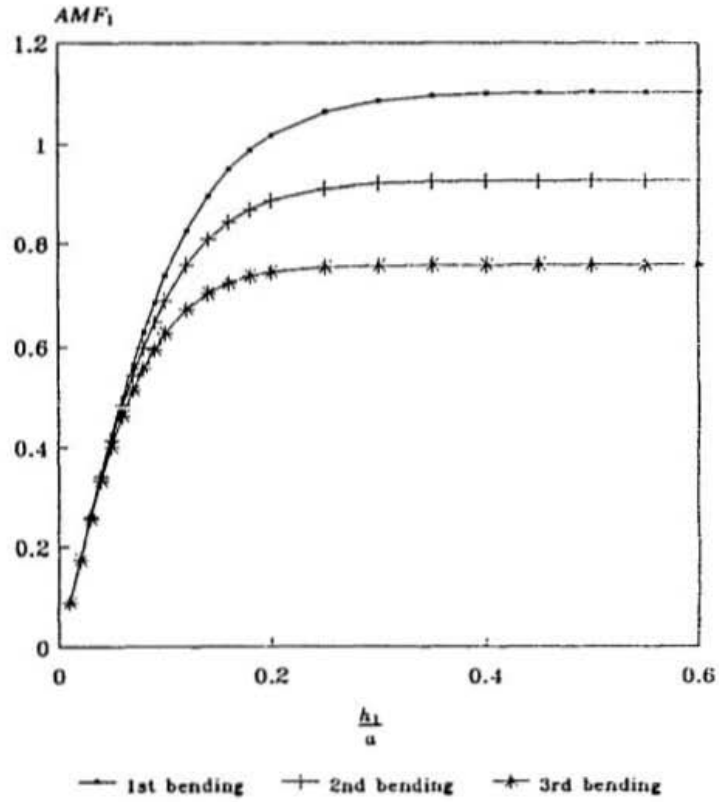

Figure 5.4: AMF_1 versus $\frac{h_1}{a}$ for the SFSF plate

AMF_1 reaches 98% its limiting value when $\frac{h_1}{a}$ is approximately 0.28, 0.22 and 0.19 for the first, second and third bending modes, respectively.

5.4.2 The Added Mass from the Fluid Field below the Submerged Plate

Similarly, the relationship between the non-dimensional added mass coefficient AMF_2 and h_2 for the CFCF and SFSF plates can be obtained using Equation 5.42, as shown in Figure 5.5 and 5.6.

Figures 5.5 and 5.6 show certain common characteristics for AMF_2 in both cases. AMF_2 decreases with the increase of the distance h_2 for all bending modes. For a value of $\frac{h_2}{a}$ greater than about 0.2, AMF_2s approach to limiting values. It is so because the tank bottom effect on the vibrating plate diminishes with the increase of the distance between them.

In addition, AMF_1 and AMF_2 have the same limiting values for the corresponding mode of plates. This fact indicates that free fluid surface and the water tank bottom have equal effect on the submerged plate when it is far from these boundaries.

5.4.3 Total Added Mass of the Plates

If $h_2 = 275$ mm, which is the same value as that in the experimental study, AMF_2 can be estimated by using Equation 5.42, which corresponds to the partial submersion case when h_1 is zero. This, together with the values of AMF_1 in Figures 5.3 and 5.4, gives the total added mass factor for the CFCF and SFSF plates submerged at different depths, as shown in Table 5.2.

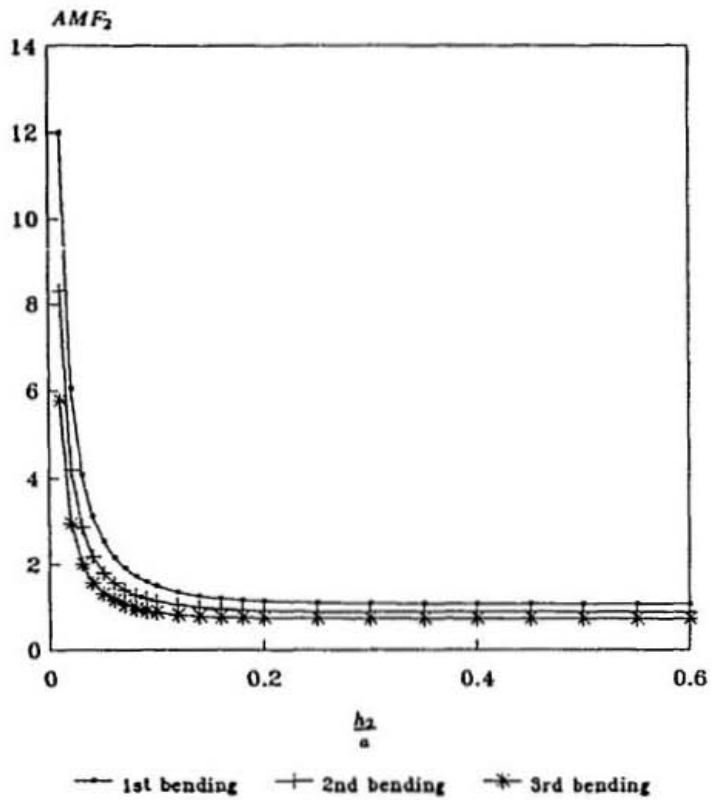

Figure 5.5: AMF_2 versus $\frac{h_2}{a}$ for the CFCF plate

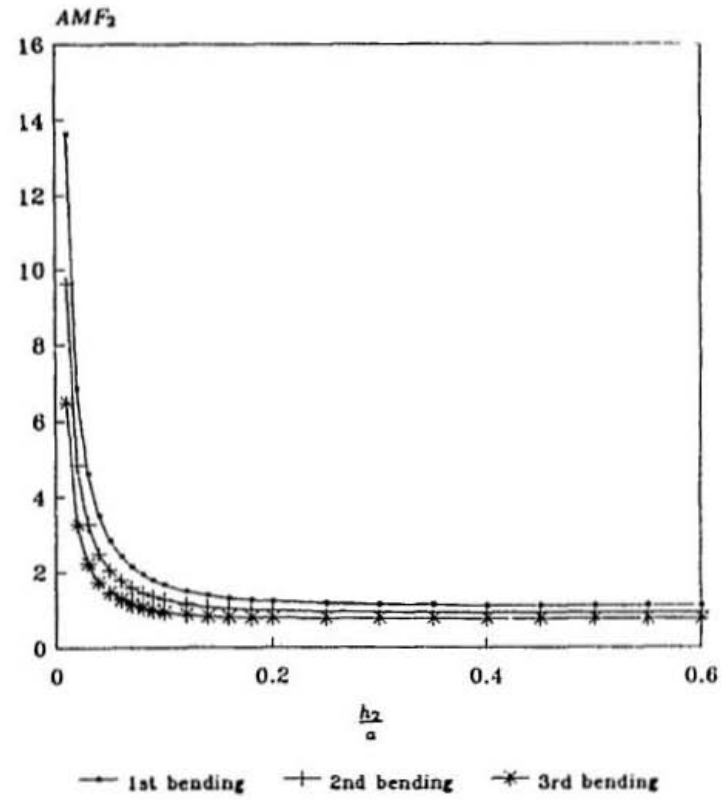

Figure 5.6: AMF_2 versus $\frac{h_2}{a}$ for the SFSF plate

Table 5.2: Predicted added mass factors for the CFCF and SFSF Plates in water

		CFCF plate			*SFSF plate*		
Mode		1st †bd.	2nd bd.	3rd bd.	1st bd.	2nd bd.	3rd bd.
Partial submergence		1.03366	0.85921	0.71527	1.10104	0.92606	0.75880
Full submergence	‡ 0.01	1.12258	0.91804	0.80395	1.19299	1.01193	0.84751
	0.02	1.21019	1.03499	0.88995	1.28079	1.10217	0.93388
	0.03	1.29526	1.11833	0.97090	1.36634	1.18629	1.01569
	0.04	1.37670	1.19663	1.04497	1.44866	1.26598	1.09126
	0.05	1.45360	1.26881	1.11104	1.52693	1.34024	1.15946
	0.06	1.52529	1.33422	1.16862	1.60049	1.40838	1.21973
	0.07	1.59133	1.39254	1.21780	1.66888	1.47003	1.27200
	0.08	1.65149	1.44383	1.25911	1.73184	1.52509	1.31661
	0.09	1.70576	1.48837	1.29330	1.78926	1.57371	1.35416
	0.10	1.75426	1.52664	1.32126	1.84118	1.61620	1.38539
	0.12	1.83510	1.58673	1.36209	1.92932	1.68467	1.43215
	0.14	1.89699	1.62906	1.38815	1.99854	1.73466	1.46302
	0.16	1.94339	1.65827	1.40447	2.05180	1.77039	1.48299
	0.18	1.97763	1.67814	1.41457	2.09214	1.79556	1.49576
	0.20	2.00261	1.69152	1.42078	2.12233	1.81309	1.50385
	0.25	2.03870	1.70862	1.42769	2.16774	1.83668	1.51328
	0.30	2.05431	1.71476	1.42969	2.18859	1.84584	1.51621
	0.35	2.06097	1.71694	1.43026	2.19800	1.84936	1.51712
	0.40	2.06379	1.71772	1.43043	2.20221	1.85071	1.51740
	0.45	2.06498	1.71799	1.43048	2.20409	1.85123	1.51749
	0.50	2.06548	1.71809	1.43049	2.20493	1.85142	1.51751
	0.60	2.06578	1.71814	1.43049	2.20547	1.85153	1.51753
	0.70	2.06584	1.71814	1.43049	2.20558	1.85154	1.51753
	0.80	2.06584	1.71814	1.43049	2.20560	1.85155	1.51753
	0.90	2.06585	1.71814	1.43049	2.20560	1.85155	1.51753
	1.00	2.06585	1.71814	1.43049	2.20560	1.85155	1.51753

†bd.-bending mode; ‡$\frac{h_1}{a}$.

5.5 Comparison between Experimental and Analytical Results

Figure 5.7 and 5.8 show the comparison between the analytical and experimental studies on the added mass factors, where "ana." and "exp." mean the results obtained by the analytical method and the experimental method, respectively; the values coinciding with $\frac{h_1}{a} = 0$ correspond to the cases of partial submergence. It is found that both analytical and experimental studies are in good agreement. However, small discrepancy does exist. The deviation between the measured and predicted added mass factor is calculated using

$$\frac{AMF^e - AMF^a}{AMF^e} \times 100\%$$

and tabulated in Table 5.3, where AMF^e and AMF^a are the added mass factor obtained by experimental and analytical method, respectively.

Table 5.3 shows that the deviation of the SFSF plate is generally greater than that of the CFCF plate, and the largest deviation is 7.916% which occurs for the SFSF plate. The discrepancy is mainly attributed to the divergence in boundary conditions of both plates and fluid between the analytical and experimental studies. Possible reasons to cause the discrepancy are:

(i) As stated earlier, any decrease in the actual support rigidity due to support strains from the infinite value assumed in the analytical method or slippage at the fixed ends will lead to a decrease in natural frequencies. This error is brought in by the manufacturing of the CFCF and SFSF plates.

(ii) The plate area is smaller than the fluid surface in the experiment study. The

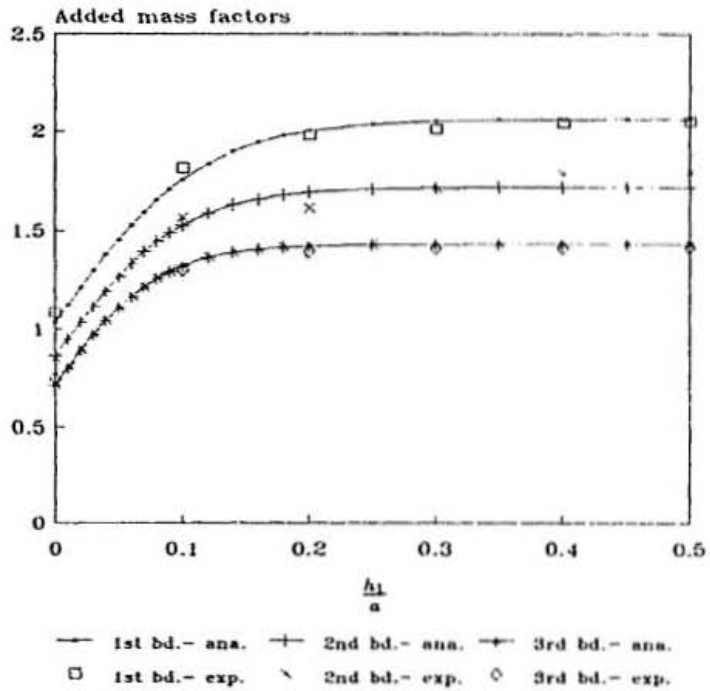

Figure 5.7: Comparison of added mass factors for the CFCF plate in water

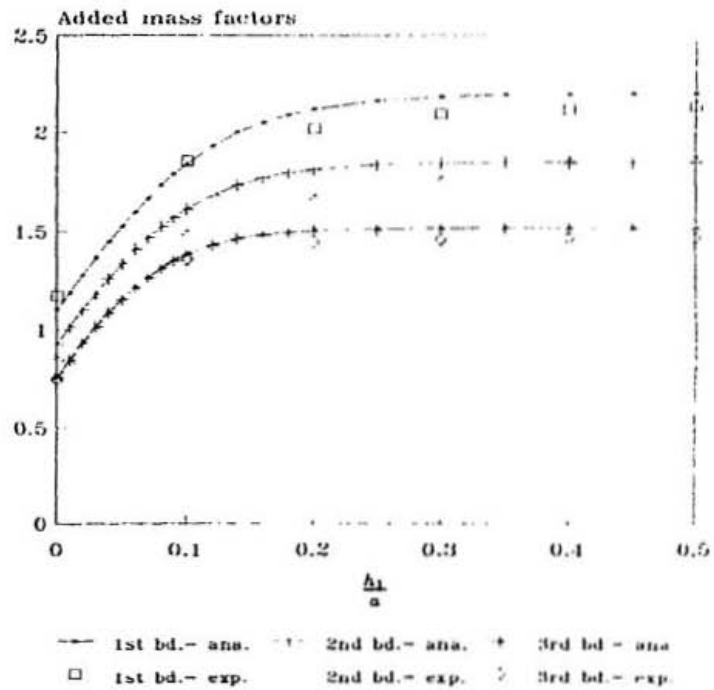

Figure 5.8: Comparison of added mass factors for the SFSF plate in water

Table 5.3: Deviation between analytical and experimental study on added mass factors

Mode			1st †bd.	2nd bd.	3rd bd.
CFCF plate	*Partial submergence*		4.679	-1.502	4.119
	Full submergence	‡0.10	3.256	2.470	-1.534
		0.20	-1.275	-4.959	-2.251
		0.30	-2.189	-0.214	-1.361
		0.40	-0.939	3.742	-1.348
		0.50	-0.677	4.173	-1.116
SFSF plate	*Partial submergence*		5.749	-7.553	-1.106
	Full submergence	0.10	0.815	-7.625	-1.770
		0.20	-5.290	-7.916	-4.037
		0.30	-4.403	-4.238	-4.000
		0.40	-3.878	0.825	-3.414
		0.50	-3.188	1.110	-3.330

†bd.-bending mode; ‡$\frac{h_1}{a}$.

analytical solution presented in this study, however, basically assumes that the plate has the same area as the surface of the fluid.

(iii) The side wall boundary conditions in fluid are not fully satisfied.

(iv) The assumption of inviscid fluid, irrotational motion and linear waves in the analytical study is only an approximation.

(v) The unavoidable noise involved in the experimental study is another reason to cause the discrepancy.

5.6 Summary

The solution to a vibrating plate loaded by fluid on two sides is presented. The general linearized fluid free surface boundary condition is applied. The relationship between the added mass due to the fluid-loading effect and the depth of submergence above and below the plate is established.

The presented analytical solution is applied to the CFCF and SFSF plates. The comparison between the analytical and experimental studies on the added mass factors of the CFCF and SFSF plates submerged in water is made, and the good agreement between them is observed. The biggest discrepancy is 7.916%, which occurs to the SFSF plate.

Chapter 6

Conclusions

When a structure vibrates in fluid, the interaction between the structure and fluid results in a decrease in the natural frequencies and an increase in the damping ratios of the vibrating structures. This thesis has investigated the fluid-plate interaction problem using analytical and experimental methods.

In the experimental study, a notched plate with clamped ends was used to simulate the simple support in the SFSF plate, and finite element software ABAQUS was used to optimize the dimensions of the notch. Experiments were carried out on the CFCF and SFSF plates both in air and in water at six different depths of submergence, respectively. For the experimental study on plates in air, the obtained natural frequencies of the plates were compared with that from the finite element program ABAQUS. The maximum deviation of 15.797% was observed in the CFCF plate. It was concluded that the notched plate with a clamped end is a good approach to the SFSF plate, and tested plates were good models of the CFCF and SFSF plates.

For the experimental study on plates in water, it was observed that due to the presence of the fluid, natural frequencies of submerged vibrating plates decreased and modal damping ratios increased. However, mode shapes did not show discernible

changes. The added mass factor and the increase in modal damping ratios of the two plates due to the presence of the fluid were evaluated for the first five modes. The effect of plate boundary conditions on the vibration of the plates in water was also investigated. Conclusions drawn from the experimental study are:

(i) Added mass factors and damping ratios increase with the increase of the depth of submergence for all modes; however, they approach limiting values with the increase in the depth of submersion.

(ii) Both added mass factors and damping rations have strong dependence on the mode shape type.

(iii) Added mass factors have dependence on the mode orders.

(iv) Both free fluid surface and the water tank bottom have approximately the same effect on the submerged plate when the vibrating plate is far from these boundaries.

Analytically, the solution to a vibrating rectangular plate loaded by fluid on two sides was presented. The general linearized fluid free surface boundary condition was applied. The relationship between the added mass due to the fluid-loading effect and the depth of submergence was established. In seeking the analytical solution, the following assumptions were made: (i) the plate undergoes a small-amplitude bending vibration and results in a small-amplitude wave motion in the fluid; (ii) the fluid is homogeneous, incompressible, inviscid and its motion is irrotational; (iii) the dynamic loading of the fluid has an insignificant effect on mode shapes; (iv) the plate field in the x-y plane has the same size as that of the fluid surface.

The presented analytical solution were applied to the CFCF and SFSF plates. A good agreement between the analytical and experimental studies on the added mass factors for the two plates in water was obtained. This demonstrates that the presented analytical solution can be used to predict the fluid effect on the natural frequencies of rectangular plates submerged in fluid at different depths.

Reference

Allemang, R.J., 1987, *"Experimental modal analysis"* , Shock and vibration handbook, McGraw-Hill Inc..

Barone, A. and Gallego-Juarez, J. A., 1972, *"Flexural vibrating free-edge plates with stepped thicknesses for generating high directional ultrasonic radiation,* "Journal of the Acoustical Society of America, Vol. 51, pp. 953-959.

Brüel & Kjær Inc., 1987, *"Instruction manual of B&K 2034 dual channel signal analyzer"*, Vol. 1 and 2.

Budipriyanto, A., 1993, *"Modal testing and analysis of uncracked and cracked plates in air and in water",* M. Eng. thesis, Memorial University of Newfoundland, St.John's, Canada.

Chowdhury, P.C., 1972, *"Fluid finite elements for added mass calculations,* " International Ship Building Progress, Vol. 19, pp. 302-309.

Davies, H. G., 1971, *"Low frequency random excitation of water-loaded rectangular plates.* " Journal of Sound and Vibration, Vol. 15, pp. 107-126.

De Santo, D.F., 1981, *"Added mass and hydrodynamic damping of perforated plates*

vibrating in water, " Journal of Pressure Vessel Technology, Vol. 103, pp. 175-182.

Donnell, L. H., 1976, *"Beams, plates and shells,* " McGraw-Hill Inc..

Dowell, E. H. and Voss, H. M., 1963, *"The effect of a cavity on panel vibration,* "American Institute of Aeronautics and Astronautics Journal, Vol. 1, pp. 476-477.

Espinosa, F. M. and Gallego-Juarez, J. A., 1984, *"On the resonance frequencies of water-loaded circular plates,* "Journal of Sound and Vibration, Vol. 94, pp. 217-222.

Everstine, G.C., 1991, *"Prediction of low frequency vibrational frequencies of submerged structures,* " Journal of Vibration and Acoustics, Vol. 113, April, pp. 187-190.

Ewins, D.J., 1984, *"Modal testing: thoery and practice"*, Research Studies Press Ltd.

Fu, Y. and Price, W. G., 1987, *"Interactions between a partially or totally immersed vibrating cantilever plate and the surrounding fluid,* "Journal of Sound and Vibration, Vol. 118, No.3, pp. 495- 513.

Geers, T. L., 1971, *"Residual Potential and Approximate Methods for Three-Dimensional Fluid-Structure Interaction Problem,* " Journal of the Acoustical Society of America, Vol. 49, pp. 1505-1510.

Gorman, D.J., 1982, *"Free Vibration Analysis of Rectangular Plates,* " New York, Elsevier Science Publishers.

Hibbitt, Karlsson & Sorensen, Inc.. 1992, *"ABAQUS user's manual"*.

Hylarides, S. and Vorus, W.S., 1982, *"The added mass matrix in ship vibration, using a sparse distribution related to the finite element grid of the ship structure."* International Shipbuilding Progress, Vol. 29, pp. 34-43.

Jezequel L., 1983, *"Hydrodynamic added mass identification from resonance tests,* "AIAA Journal, Vol. 21, No.4, pp. 608-613.

Junger, M. and Feit, D., 1972, *" Sound, Structures and Their Interaction,* " Cambridge, Mass., MIT Press.

Kundu, P.K., 1990, *"Fluid mechanics"*, Academic Press Inc..

Kwak, M. K. and Kim, M. K., 1991, *"Axisymmetric Vibration of Circular Plates in Contact with Fluid,* " Journal of Sound and Vibration, Vol. 146, pp. 381-389.

Lamb, H., 1921, *"On the vibrations of an elastic plate in contact with water,* " Proceedings of the Royal Society of London, Series A 98, pp. 205-216.

Leibowitz, R. C., 1975, *"Vibroacoustic Response of Turbulence Excited Thin Rectangular Finite Plates in Heavy and Light Fluid Media,* "Journal of Sound and Vibration, Vol. 40(4), pp. 441-495.

Lindholm, U. S., Kana, D. D., Chu, Wen-Hwa, and Abramson, H. N., 1965, *"Elastic*

vibration characteristics of cantilever plates in water, " Journal of Ship Research, June, pp. 11-22.

McLachlan, N. W., 1932, "*The accession to inertia of flexible discs vibrating in a fluid,* " Proceedings of the Physical Society, (London) Vol. 44, pp. 546-555.

Muthuveerappan, G. and Veluswami, M.A., 1978, " *Vibration of square cantilever plate immersed in water,* "Journal of Sound and Vibration, Vol. 61, No.3, pp. 476-470.

Muthuveerappan, G., Ganesan, N. and Veluswami, M.A., 1979, "*A note on vibration of cantilever plate immersed in water,* " Journal of Sound and Vibration, Vol. 63, No.3, pp. 385-391.

Muthuveerappan, G., Ganesan, N. and Veluswami, M.A., 1980, "*Influence of fluid added mass on the vibration characteristics of plates under various boundary conditions,* " Journal of Sound and Vibration, Vol. 69, No.4, pp. 612-615.

Peake, W. H. and Thurston, E. G., 1954, "*The lowest resonant frequency of a water-loaded circular plate,* " Journal of the Acoustical Society of America, Vol. 26, pp. 166-168.

Powell, J. H. and Roberts, J. H., 1923, "*On the frequency of vibration of circular diaphragms,* "Proceedings of the Physical Society(London), Vol. 35, pp. 170-182.

Pretlove, A.J., 1965. *"Free vibrations of a rectangular panel backed by a closed rectangular cavity,"* Journal of Sound and Vibration, Vol. 2, pp. 197-209.

Qaisi, M.I., 1988, *"Free vibrations of a rectangular plate-cavity system,"* Applied Acoustics, Vol. 24, pp. 49- 61.

Randall, L.R., 1985, *"Modal analysis of a cylindrical structure immersed in water"*, Proceedings of the third international modal analysis conference, Vol. 2, pp. 738-744.

Rayleigh, L., 1877, *" Theory of Sound, "* New York, Dover publications, second edition, 1945 re-issue.

Robinson, N. J. and Palmer, S. C., 1990, *"A modal analysis of a rectangular plate floating on an incompressible liquid,"* Journal of Sound and Vibration, Vol. 142(3), pp. 453-460.

Structural Measurement Systems, 1990, *"STAR: theory of operation"*.

Structural Measurement Systems, 1992, *"STAR: advanced curve fitting reference manual"*.

Appendix A

Derivation of Equations 5.20 and 5.21

As stated earlier, a separable solution to the bending displacement of a plate and the velocity potential in fluid can be sought in this study, i.e.,

$$W(x,y,t) = \overline{W}(x,y)T(t) \tag{A.1}$$

$$\phi(x,y,z,t) = G(x,y)F(z)S(t) \tag{A.2}$$

Then

$$\frac{\partial^2 W}{\partial t^2} = \overline{W}\frac{d^2T}{dt^2} = \overline{W}\ddot{T} \tag{A.3}$$

By applying Equations 5.18 and 5.19, one has

$$\frac{\partial \phi}{\partial t}\mid_{z=-(h_1+h)} - \frac{\partial \phi}{\partial t}\mid_{z=-h_1} = \overline{W}\ddot{T}[\frac{F}{F'}\mid_{z=-(h_1+h)} - \frac{F}{F'}\mid_{z=-h_1}] \tag{A.4}$$

$$\nabla^4 W = T\nabla^4\overline{W} \tag{A.5}$$

Applying Equations A.3,A.4 and A.5 to Equation 5.10 gives

$$m\overline{W}\ddot{T} + \rho_f[\frac{F}{F'}\mid_{z=-(h_1+h)} - \frac{F}{F'}\mid_{z=-h_1}]\overline{W}\ddot{T} + DT\nabla^4\overline{W} - \rho_f g h = 0 \tag{A.6}$$

where the term $\rho_f gh$ is a static load. it has effect only on the equilibrium position, but not on the dynamical response. So Equation A.6 can be solved without considering this static term.

Consider the equation

$$m\overline{W}\ddot{T} + \rho_f[\frac{F}{F'}\,|_{z=-(h_1+h)} - \frac{F}{F'}\,|_{z=-h_1}]\overline{W}\ddot{T} + DT\nabla^4\overline{W} = 0 \qquad (A.7)$$

that is,

$$(m + m^*)\overline{W}\ddot{T} + DT\nabla^4\overline{W} = 0 \qquad (A.8)$$

where

$$m^* = \rho_f[\frac{F}{F'}\,|_{z=-(h_1+h)} - \frac{F}{F'}\,|_{z=-h_1}] \qquad (A.9)$$

In the Equation A.8, $\overline{W}(x, y)$ and $T(t)$ are, respectively, functions of position and time only, so the following relationship holds

$$-\frac{\ddot{T}}{T} = \frac{1}{c^2}\frac{\nabla^4\overline{W}}{\overline{W}} = \omega_{fluid}^2 \qquad (A.10)$$

that is,

$$\ddot{T} + \omega_{fluid}^2 T = 0 \qquad (A.11)$$

$$\nabla^4\overline{W} - \beta^4\overline{W} = 0 \qquad (A.12)$$

where

$$c^2 = \frac{m + m^*}{D}$$

$$\beta^4 = \omega_{fluid}^2 c^2 = \frac{\omega_{fluid}^2(m + m^*)}{D} \qquad (A.13)$$